Article:

Song, X-G, Yang, H, Yue, H-Y et al. (3 more authors) (2022) Closed-form solutions for large strain analysis of cavity contraction in a bounded Mohr-Coulomb medium. European Journal of Environmental and Civil Engineering, 26 (10). pp. 4548-4575. ISSN 1964-8189

https://doi.org/10.1080/19648189.2020.1857309

Closed-form solutions for large strain analysis of cavity contraction in a bounded Mohr-Coulomb medium

Xiu-Guang Song [1 a], He Yang [1 b], Hong-Ya Yue [1,3 c],

Xu Guo [2 d], Hai-Sui Yu [3 e], Pei-Zhi Zhuang [*1,3]

[1] *School of Qilu Transportation, Shandong University, Jinan, 250002, China*

[2] *Geotechnical and Structural Engineering Research Center, Shandong University, Jinan, 250061, China*

[3] *School of Civil Engineering, University of Leeds, LS2 9JT Leeds, UK*

[*]Corresponding author, Research fellow, E-mail: p.zhuang@leeds.ac.uk

[a] Professor, E-mail: songxiuguang@sdu.edu.cn

[b] Master student, E-mail: yanghesdu@mail.sdu.edu.cn

[c] Ph.D. candidate, E-mail: yuehongya@mail.sdu.edu.cn

[d] Professor, E-mail: guoxu1014@163.com

[e] Professor, E-mail: h.yu@leeds.ac.uk

Abstract: This paper presents rigorous analytical solutions for cavity contraction analysis of a thick-walled cylinder/sphere after an arbitrary magnitude of expansion. Closed-form solutions are given for the distribution of stress and displacement within the cylinder/sphere of soil that is subjected to constant external pressure and monotonically decreasing internal pressure. The soil is modelled as an elastic-perfectly plastic material obeying the Mohr-Coulomb yield criterion and a non-associated flow rule. Large strain effects are taken into account by adopting the logarithmic strain definition in the plastic deformation analysis. The new solutions are validated with published results at first, then parametric studies are carried out. It is shown that the reference stress state (e.g. in-situ, elastic, partially plastic and fully plastic) and the cavity geometry ratio may greatly affect the unloading behaviour, in particular, when the cavity geometry ratio is smaller than a limit value. Finally, three typical applications of the solutions are demonstrated, including (i) design of the thickness of frozen cylinder walls accounting for large deformation effects, (ii) interpretation of laboratory pressuremeter tests with consideration of effect of the constant stress boundary, and (iii) shakedown analysis of a soil cylinder/sphere considering its geometry changes upon cyclic loading and unloading.

Keywords: Cavity contraction; Boundary effect; Shakedown; Pressuremeter; Frozen earth wall

Introduction

Cavity contraction theory is concerned with the theoretical study of changes in stresses and displacements of cylindrical and spherical cavities upon unloading. It provides a versatile and accurate tool for study of a variety of geotechnical problems. Among them are the interpretation of pressuremeter tests (Ferreira & Robertson, 1992; Houlsby et al., 1985; Houlsby & Withers, 1988; Jefferies, 1988; Schnaid et al., 2000; Shuttle, 2007; Withers et al., 1989; Yu, 1996) and analysis of stability and deformation associated with underground excavation, tunneling and drilling (Brown et al., 1983; Carter, 1988; Chen et al., 2012; Jirari et al., 2020; Mair & Taylor, 1993; Mo & Yu, 2017; Ogawa & Lo, 1987; Vrakas & Anagnostou, 2014; Yu & Rowe, 1999). In the modelling of pressuremeter tests during unloading, the cavity contraction analysis normally starts from a residual (elastic-plastic) stress state that was induced by previous loading (e.g. installation and expansion of pressuremeters). However, it is usually assumed that the soil is unloaded from an in-situ elastic stress state in the stability and deformation analysis of tunnels and wellbores. Hence, corresponding cavity contraction analyses involve different complexity. Both cases will be considered in this study.

Cavity contraction approaches for modelling pressuremeter tests were advocated mainly because the unloading response of pressuremeters is less sensitive to the initial soil disturbance (Hughes & Robertson, 1985; Schnaid & Houlsby, 1992). Over the years, a number of solutions has been developed to derive soil properties from the unloading portion of pressuremeter curves for both sand (Houlsby et al., 1985; Schnaid et al., 2000; Withers et al., 1989; Yu, 1996) and clay (Ferreira & Robertson, 1992; Houlsby & Withers, 1988; Jefferies, 1988). For example, assuming the cavity unloading from the limit expansion state, Houlsby and Withers (1988) derived an analytical solution for both cylindrical and spherical cavities in clays obeying the Tresca failure criterion. Using a non-associated Mohr-Coulomb plasticity model, Houlsby et al. (1985) first developed an approximate small strain solution for interpreting the unloading portion of pressuremeter curves in sands, which was extended later by Withers et al. (1989) to include the case of a spherical cavity. Later on, Yu and Houlsby (1995) presented a more rigorous large-strain solution for the analysis of unloading from any elastic-plastic stress state adopting the same soil model. These unloading solutions are also of great importance for the interpretation methods that consider both the loading and unloading portions of pressuremeter tests (Jefferies, 1988; Schnaid et al., 2000). Nevertheless, almost without exception, the previous analytical solutions for elastic-plastic contraction analysis have been developed with the idealization that the surrounding soil is infinitely large. This assumption may approximately represent the field conditions of site pressuremeter tests but is not suitable for tests performed in small-sized containers due to the possible lateral boundary effects (Alsiny et al., 1992; Fahey

& Carter, 1993; Geng et al., 2012; Jewell et al., 1980; Schnaid & Houlsby, 1991). To capture the boundary effects, many analytical/semi-analytical expansion solutions for cavities within a bounded soil mass have been proposed (Cheng & Yang, 2019; Fahey, 1986; Juran & BenSaid, 1987; Pournaghiazar et al., 2013; Salgado et al., 1998; Yu, 1992, 1993). However, the progress in developing counterpart contraction solutions in bounded soils lags much behind due to the presence of residual stresses that makes the mathematics of the unloading analysis more complex than that of loading. Existing elastic-plastic loading-unloading studies into this problem mainly focused on the shakedown behaviour of a thick-walled cylinder or sphere, which usually involves elastic unloading only and is lack of consideration for the deformation (Gao et al., 2015; Hill, 1950; Wen et al., 2017; Xu & Yu, 2005; Zhao & Wang, 2010).

Cavity contraction analysis from an in situ stress state can be regarded as a reverse process of traditional cavity expansion analysis (Chadwick, 1959; Collins & Yu, 1996; Yu & Rowe, 1999). As such, the solution methods between them are transferable. Meanwhile, the elastic initial stress state is relatively simple. Hence, many relevant analytical/semi-analytical contraction solutions have been developed in this case over the years (Brown et al., 1983; Chen & Abousleiman, 2016; Mo & Yu, 2017; Park, 2014; Sharan, 2008; Vrakas & Anagnostou, 2014; Yu & Rowe, 1999; Yu et al., 2019). Likewise, most of them concentrated on the case of a cavity embedded in an infinite soil mass, which represents a reasonable simplification for the problem of deep tunnels and un-reinforced boreholes. However, this is not suitable for the unloading analysis of thick-walled soil cylinders or shallow tunnels (Abdulhadi et al., 2011; Franza et al., 2019; Grant, 1998; Mair, 1979), for example, in the stability and deformation analysis of controlled ground freezing involved tunnels and boreholes, in which the finite thickness of the frozen earth wall must be well accounted for (Andersland & Ladanyi, 2004; Sanger & Sayles, 1979; Zhang et al., 2018).

In this paper, we present analytical large strain solutions for contraction analysis of a thick-wall cylinder/sphere of dilatant elastic-plastic soils using the Mohr-Coulomb yield criterion and a non-associated flow rule. Without loss of generality, an arbitrary residual stress state (including in-situ, elastic, partially plastic and fully plastic) induced by loading prior to the unloading is considered. The solutions at first are compared with other solutions in the special case of an infinite soil mass for validation. This is followed by parametric studies with a focus on the effects of soil thickness and loading history on cavity contraction behaviour. Finally, three typical applications of the new solutions are presented to show their usefulness, including (i) preliminary design of the thickness of frozen cylinder walls, (ii) prediction of pressuremeter curves measured in calibration chambers in sand, and (iii) determination of the optimal thickness of a hollow cylinder/sphere based on the shakedown concept considering the large deformation effects.

Problem definition and reference stress state

Problem definition

Initially, the inner and outer radii of the soil cylinder/sphere are a_0 and b_0, respectively, and a hydrostatic pressure p_0 acts throughout the soil which is assumed to be isotropic and homogeneous. An additional radial pressure $p_{\mathrm{in}} - p_0$ (≥ 0) is then applied at the inner wall of the cavity and increased gradually (i.e. loading). At the end of the loading process (i.e. $p_{\mathrm{in}} = p_{20}$), the inner and outer radii of the cylinder/sphere are a_{20} and b_{20}, respectively. Subsequently, the radial pressure acting on the inner cavity wall reduces monotonically (i.e. unloading). During the loading and unloading processes, the internal cavity pressure is applied or removed sufficiently slowly, thus the dynamic effects are negligible, and the radial confining pressure at the outer wall of the cavity remains unchanged as p_0. The major concern of this paper is the distribution of stress and displacement in the cylinder/sphere of soil during the unloading process.

The unloading analyses of cylindrical and spherical cavities are conducted simultaneously by the introduction of a parameter k which takes 1 for a cylindrical cavity and 2 for a spherical cavity. For convenience, the behaviour of the cylindrical cavity is described in terms of cylindrical polar coordinates (r, θ, z) and the behaviour of the spherical cavity is described in terms of spherical polar coordinates (r, θ, ϕ). As a long cylindrical cavity is considered, its expansion and contraction occur under plane strain conditions with respect to the z-direction of the cylindrical coordinates.

Under axisymmetric/spherically-symmetric conditions, the equilibrium equation in the radial direction can be expressed as:

$$\frac{\mathrm{d}\sigma_r}{\mathrm{d}r} + \frac{k}{r}\left(\sigma_r - \sigma_\theta\right) = 0 \tag{1}$$

where σ_r and σ_θ represent the radial and circumferential stresses, respectively.

The configuration of the system at the completion of loading is used as a reference state from which the stress and displacement of the unloading process are measured. For clarity, subscripts '0', '1' and '2' are used in this paper to distinguish the in-situ (or initial) state, the loading process and the unloading process (e.g. Figure 1). The residual stresses and radial displacement during unloading are expressed as:

$$\sigma_{r2} = \sigma_{r20} + \Delta\sigma_r \tag{2}$$

$$\sigma_{\theta 2} = \sigma_{\theta 20} + \Delta\sigma_\theta \tag{3}$$

$$u_2 = u_{20} + \Delta u = r_2 - r_0 \tag{4}$$

where σ_{r2}, $\sigma_{\theta 2}$ and u_2 represent radial stress, circumferential stress, and radial displacement during unloading, and σ_{r20}, $\sigma_{\theta 20}$ and u_{20} represent their values at the end moment of loading (or beginning of unloading), respectively. $\Delta\sigma_r$, $\Delta\sigma_\theta$ and Δu are changes in the radial stress, the circumferential stress and the radial displacement due to unloading, respectively; r_2 is the radial coordinate of a soil particle during unloading, and r_0 indicates its original location.

Taking tensile as positive, the stress boundary conditions during unloading are defined as:

$$\sigma_{r2}\big|_{r_2=a_2} = -p_2 \quad , \quad \sigma_{r2}\big|_{r_2=b_2} = -p_0 \tag{5 a,b}$$

The surrounding soil is modelled as a linearly elastic-perfectly plastic material obeying the Mohr-Coulomb criterion and a non-associated flow rule. The soil behaves elastically and obeys Hooke's law until the onset of yielding. Depending on the loading history, possible reference stress states within the finite soil medium at the beginning of unloading can be generally divided into three cases as shown in Figure 1, namely (I) purely elastic state (including the case of $p_{20} = p_0$); (II) partially plastic state; and (III) fully plastic state. In Figure 1, c_1 denotes the radius of the elastic-plastic boundary during the loading phase, c_{20} represents its value at the end of loading (or the beginning of unloading), and c_2 denotes the outer radius of the loading-induced plastic zone during unloading. Note that the axial stress σ_z in the cylindrical case is assumed to be the intermediate principal stress for the sake of analytical solutions, and it has been shown that the errors that may be caused in the associated stress and displacement fields by this simplification are negligible for practical purpose (Reed, 1986; Vrakas & Anagnostou, 2014).

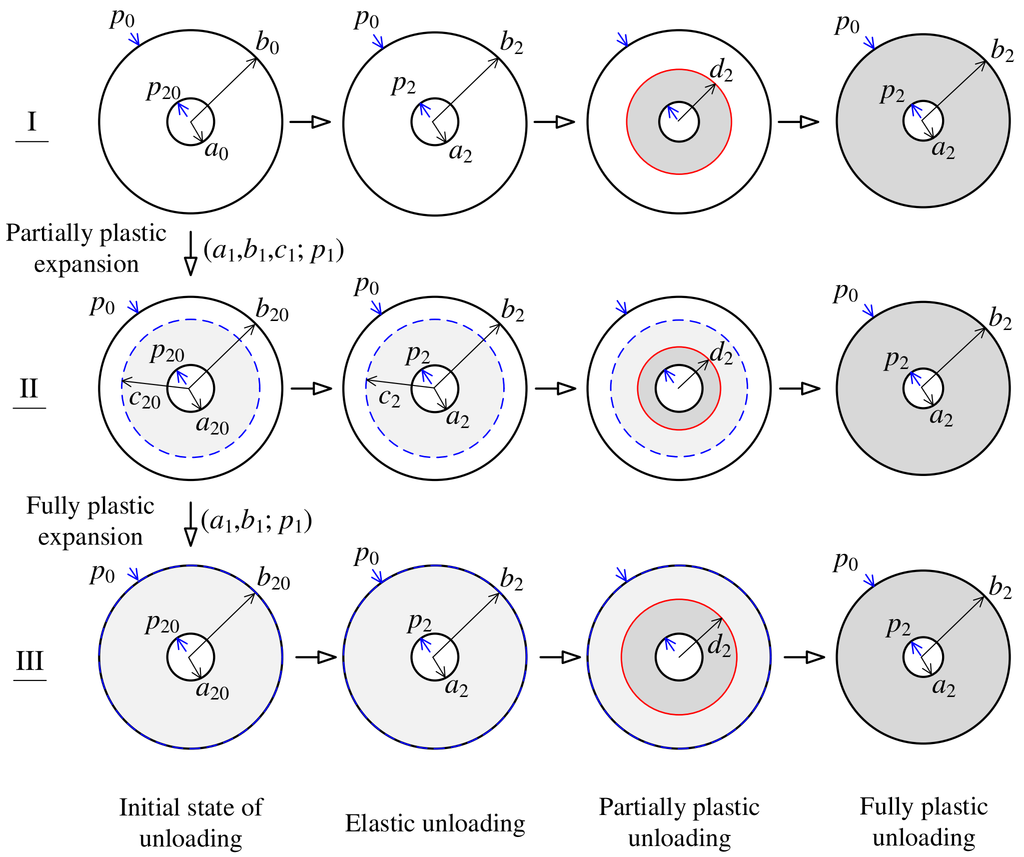

Figure1. Definition of the loading and unloading processes

As the cavity pressure p_2 reduces from p_{20}, the surrounding soil contracts purely elastically at first (i.e. the elastic unloading phase in Figure 1). With further removal of the internal pressure, plastic yielding occurs in the reverse direction (referred to as 'reverse yielding') once the residual stresses satisfy the Mohr-Coulomb yielding criterion under unloading, which initiates from the inner wall of the cavity (i.e. the partially plastic unloading phase in Figure 1). The outer radius of the reverse plastic zone is denoted as d_2, and its corresponding position at the fully loaded state (i.e. the reference state) is denoted as d_{20}. Upon further unloading, the entire soil annulus or spherical shell may enter the plastic state (i.e. fully plastic unloading phase in Figure 1). In the reverse plastic zone, the circumferential stress becomes the major principle stress and the yielding function can be expressed as:

$$\alpha\sigma_{r2} - \sigma_{\theta 2} = Y \tag{6}$$

where $\alpha = (1+\sin\varphi)/(1-\sin\varphi)$; $Y = 2c\cos\varphi/(1-\sin\varphi)$. φ is the angle of friction and c is the cohesion of soil. It has been proven that Equation (6) is satisfied throughout the whole unloading process for any soil (Vrakas & Anagnostou, 2014; Yu & Houlsby, 1995).

Reference stress state for unloading

The soil model adopted in this study is the same as that was used by Yu (1992, 1993) in the loading analysis of a cylinder/sphere. At first, following Yu (1992, 1993), the distribution of stress in the soil during loading is presented to provide a reference for the analysis of the subsequent unloading process.

Upon uniform and monotonic loading, the surrounding soil behaves elastically before the cavity pressure reaches the elastic limit $p_{1\text{elim}}$, and the distribution of the elastic stresses is known as:

$$\sigma_{r1} = -p_0 - (p_1 - p_0)\frac{(b_1/r_1)^{k+1} - 1}{(b_1/a_1)^{k+1} - 1} \tag{7}$$

$$\sigma_{\theta 1} = -p_0 + (p_1 - p_0)\frac{\left[(b_1/r_1)^{k+1}\right]/k + 1}{(b_1/a_1)^{k+1} - 1} \tag{8}$$

$$p_{1\text{elim}} = p_0 + \frac{\left[Y + (\alpha - 1)p_0\right]\left[(b_1/a_1)^{k+1} - 1\right]}{(\alpha / k + 1)(b_1/a_1)^{k+1} + \alpha - 1} \tag{9}$$

When the cavity pressure increases to be larger than $p_{1\text{elim}}$, the distribution of stresses is defined as:

$$\sigma_{r1} = Y/(\alpha - 1) - A_1 (c_1/r_1)^{\frac{k(\alpha-1)}{\alpha}} \tag{10}$$

$$\sigma_{\theta 1} = Y/(\alpha - 1) - (A_1/\alpha)(c_1/r_1)^{\frac{k(\alpha-1)}{\alpha}} \tag{11}$$

for $a_1 \le r_1 \le c_1$ (i.e. the loading plastic zone), and

$$\sigma_{r1} = -p_0 - B_1\left[(b_1/r_1)^{k+1} - 1\right] \tag{12}$$

$$\sigma_{\theta 1} = -p_0 + B_1\left[(b_1/r_1)^{k+1}/k + 1\right] \tag{13}$$

for $c_1 \le r_1 \le b_1$ (i.e. the loading elastic zone). In which,

$$A_1 = \frac{\alpha(k+1)\left[Y + (\alpha - 1)p_0\right]}{k(\alpha - 1)\left[\alpha/k + 1 + (\alpha - 1)(c_1/b_1)^{k+1}\right]} \tag{14}$$

$$B_1 = \frac{Y + (\alpha - 1) p_0}{(\alpha/k + 1)(b_1/c_1)^{k+1} + \alpha - 1} \tag{15}$$

The radius of the elastic-plastic boundary upon loading (i.e. c_1) can be determined by:

$$(c_1/a_1)^{\frac{k(\alpha-1)}{\alpha}} = \frac{\left[k(\alpha-1)(c_1/b_1)^{k+1} + \alpha + k\right]\left[Y + (\alpha-1)p_1\right]}{\alpha(k+1)\left[Y + (\alpha-1)p_0\right]} \tag{16}$$

With sufficiently large loading, the entire soil mass of a finite radial extent may become fully plastic (i.e. $c_1 = b_1$). The distribution of stress in this phase can also be determined by Equations (5 a,b), (10) and (11) by replacing c_1 with b_1 therein.

At the beginning of unloading, $a_1 = a_{20}$, $b_1 = b_{20}$ and $p_1 = p_{20}$. According to the difference in the residual stress state and the corresponding geotechnical applications, solutions for the unloading analysis from an in-situ (or elastic) stress state and a plastic reference stress state will be derived separately in the following two sections for clarity.

Solutions for unloading from an in-situ/elastic stress state

This section focuses on the analysis of a cavity unloading from an elastic stress state (namely, case I in Figure 1, $p_0 \le p_{20} \le p_{1\mathrm{elim}}$). In this case, the unloading from p_{20} back to p_0 is a reverse process of the previous elastic loading (fully recoverable). Thus, the distribution of stress and strain during this process can be readily obtained by the corresponding loading solution (e.g. (Yu, 1992, 1993)). Hence, the following analysis is carried out with reference to an *in-situ* stress state for brevity.

Elastic unloading analysis

In the elastic unloading analysis, the small strain definition (e.g. Equations (17) and (18)) is adopted as the elastic deformation is rather small (Houlsby & Withers, 1988; Yu & Houlsby, 1995). This is commonly used in quasi-static cavity expansion and contraction analyses and consistent with the counterpart expansion analysis of Yu (1992, 1993). Hence, the elastic stress-strain relationships in rate forms are:

$$\dot{\varepsilon}_r = \frac{\mathrm{d}\dot{u}_2}{\mathrm{d}r_2} = \frac{1}{M}\left(\dot{\sigma}_{r2} - \frac{kv}{1 - v(2-k)}\dot{\sigma}_{\theta 2}\right) \tag{17}$$

$$\dot{\varepsilon}_\theta = \frac{\dot{u}_2}{r_2} = \frac{1}{M}\left[\frac{-v}{1 - v(2-k)}\dot{\sigma}_r + (1 + v - kv)\dot{\sigma}_\theta\right] \tag{18}$$

where ε_r and ε_θ denote radial and circumferential strains, respectively. v is the Poisson's ratio. $M = E/\left[1-v^2(2-k)\right]$; E is the elastic modulus of soil, and E=2G(1+v); G is the shear modulus of soil.

Changes in the stresses and radial displacement due to purely elastic unloading from p_0 to p_2 can be determined by solving the stress equilibrium equation (i.e. Equation (1)) and the strain compatibility equations (i.e. Equations (17) and (18)) with the stress boundary conditions defined in Equation (5 a,b) as:

$$\sigma_{r2} = -p_0 - (p_2 - p_0)\frac{(b_2/r_2)^{k+1} - 1}{(b_2/a_2)^{k+1} - 1} \tag{19}$$

$$\sigma_{\theta 2} = -p_0 + (p_2 - p_0)\frac{(b_2/r_2)^{k+1}/k + 1}{(b_2/a_2)^{k+1} - 1} \tag{20}$$

$$u_2(r_2) = \frac{(p_2 - p_0)}{Mr_2^k\left(1/a_2^{k+1} - 1/b_2^{k+1}\right)}\left\{(1+v-kv)\left[\left(\frac{r_2}{b_2}\right)^{k+1} + \frac{1}{k}\right] + \frac{v}{1-v(2-k)}\left[1 - \left(\frac{r_2}{b_2}\right)^{k+1}\right]\right\} \tag{21}$$

Equations (19) and (20) show that σ_{r2} increases and $\sigma_{\theta 2}$ decreases upon unloading. Reverse plasticity occurs once the Mohr-Coulomb yield criterion Equation (6) is satisfied. This condition is firstly satisfied at the inner wall of the cavity when the internal pressure reaches its reverse elastic limit $p_{2\mathrm{elim}-1}$:

$$p_{2\mathrm{elim}-1} = p_0 - \frac{\left[Y + (\alpha - 1)p_0\right]\left[(b_2/a_2)^{k+1} - 1\right]}{(\alpha + 1/k)(b_2/a_2)^{k+1} + 1 - \alpha} \tag{22}$$

Elastic-plastic unloading analysis

Stress analysis

As the cavity pressure p_2 further reduces, a plastic unloading zone $a_2 \le r_2 \le d_2$ forms and spreads outwards from the inner wall of the cavity. The distribution of stress in the soil can be obtained by considering the plastic zone and elastic zone (i.e. $d_2 \le r_2 \le b_2$) separately and matching at the elastic-plastic interface $r_2 = d_2$.

In the elastic zone (i.e. $d_2 \le r_2 \le b_2$), the unloading-induced changes in the principal stresses can be obtained by solving the stress equilibrium equation (i.e. Equation (1)) and the strain compatibility equations (i.e. Equations (17) and (18)) as:

$$\sigma_{r2} = -p_0 + B_{2-1}\left[\left(b_2/r_2\right)^{k+1} - 1\right] \tag{23}$$

$$\sigma_{\theta 2} = -p_0 - B_{2-1}\left[\left(b_2/r_2\right)^{k+1}/k + 1\right] \tag{24}$$

where the integration constant $B_{2\text{-}1}$ can be determined as the yield criterion of Equation (6) is satisfied at r_2=d_2, namely

$$B_{2-1} = \frac{Y + (\alpha - 1)p_0}{(\alpha + 1/k)\left(b_2/d_2\right)^{k+1} + 1 - \alpha} \tag{25}$$

In the reverse plastic zone ($a_2 \le r_2 \le d_2$), the principal stresses are determined by jointly solving the stress equilibrium equation and the Mohr-Coulomb yield criterion as:

$$\sigma_{r2} = Y/(\alpha - 1) + A_{2-1}\left(d_2/r_2\right)^{k(1-\alpha)} \tag{26}$$

$$\sigma_{\theta 2} = Y/(\alpha - 1) + \alpha A_{2-1}\left(d_2/r_2\right)^{k(1-\alpha)} \tag{27}$$

where the integration constant $A_{2\text{-}1}$ can be determined from the continuity condition of stress components at the outer radius of the elastic-plastic interface (i.e. r_2=d_2) as:

$$A_{2-1} = \frac{-(k+1)\left[Y + (\alpha - 1)p_0\right]}{k(\alpha - 1)\left[\alpha + 1/k + (1-\alpha)\left(d_2/b_2\right)^{k+1}\right]} \tag{28}$$

Then the cavity pressure p_2 and the radius of the elastic-plastic interface d_2 during unloading can be related based on Equations (5 a), (26) and (28) as:

$$\left(\frac{d_2}{a_2}\right)^{k(1-\alpha)} = \frac{k}{(k+1)}\frac{\left[Y + (\alpha - 1)p_2\right]}{\left[Y + (\alpha - 1)p_0\right]}\left[\alpha + \frac{1}{k} + (1-\alpha)\left(\frac{d_2}{b_2}\right)^{k+1}\right] \tag{29}$$

While p_2 reduces to the fully plastic limit value $p_{2\mathrm{fp-lim}}$, the entire soil medium will become plastic. Equation (29) gives:

$$p_{2\mathrm{fp-lim}} = p_0 + \frac{Y + (\alpha - 1)p_0}{\alpha - 1}\left[\left(b_2/a_2\right)^{k(1-\alpha)} - 1\right] \tag{30}$$

Displacement analysis

In the elastic unloading zone ($d_2 \le r_2 \le b_2$), the radial displacement at r_2 can be obtained by integrating Equations (17) and (18) with the inputs of Equations (23) and (24) as:

$$u_2\left(r_2\right)=\frac{-B_{2-1}r_2}{M}\left\{1+v-kv-\frac{v}{1-v\left(2-k\right)}+\left[\frac{v}{1-v\left(2-k\right)}+\frac{1+v-kv}{k}\right]\left(\frac{b_2}{r_2}\right)^{k+1}\right\} \quad (31)$$

At the elastic-plastic interface and the outer wall of the cavity, we have:

$$d_{20}=d_2-u_2\left(d_2\right) \ , \quad b_{20}=b_2-u_2\left(b_2\right) \quad (32a, b)$$

In the displacement analysis within the plastic unloading zone ($a_2<r_2<d_2$), a non-associated flow rule (i.e. ψ is not necessarily equal to φ; ψ is the dilation angle of soil) is adapted, and ψ is assumed to be constant to limit the complexity of the model so that closed-form solutions can be obtained. The non-associated flow rule is expressed as:

$$\frac{\dot{\varepsilon}_r^p}{\dot{\varepsilon}_\theta^p}=\frac{\dot{\varepsilon}_r-\dot{\varepsilon}_r^e}{\dot{\varepsilon}_\theta-\dot{\varepsilon}_\theta^e}=-k\beta \quad (33)$$

where $\beta=\left(1+\sin\psi\right)/\left(1-\sin\psi\right)$. Note that the dilatancy of soils is in fact not constant (e.g. tends to zero at critical state). Hence, the above assumption on the dilation angle may lead to overprediction on the volumetric deformation at large deformation. The superscripts '*e*' and '*p*' represent the elastic and plastic components of strain, respectively. The distribution of stress and strain in the soil at the initiation of reverse plastic yielding is known with Equations (17)-(20) by putting $p_2=p_{2\text{elim}-1}$. Subject to this initial condition, the total stress-strain relation in the reverse plastic zone is obtained by integrating Equations (17), (18) and (33) as:

$$\varepsilon_{r2}+k\beta\varepsilon_{\theta 2}=\frac{1}{M}\left\{\left[1-\frac{k\beta v}{1-v\left(2-k\right)}\right]\left(\sigma_{r2}+p_0\right)+\left[k\beta\left(1+v-kv\right)-\frac{kv}{1-v\left(2-k\right)}\right]\left(\sigma_{\theta 2}+p_0\right)\right\} \quad (34)$$

The definition of logarithmic strain is adopted to account for the effects of large strain in the axisymmetric plastic deformation analysis (Chadwick, 1959; Yu & Houlsby, 1995), namely:

$$\varepsilon_{r2}=\ln\left(\mathrm{d}r_2/\mathrm{d}r_0\right) \ , \quad \varepsilon_{\theta 2}=\ln\left(r_2/r_0\right) \quad (35\text{ a,b})$$

Substituting Equations (10), (11), (26), (27) and (35 a,b) into Eq. (34) leads to:

$$\ln\frac{r_2^{k\beta}\mathrm{d}r_2}{r_0^{k\beta}\mathrm{d}r_0}=\ln\eta-\omega\left(d_2/r_2\right)^{k(1-\alpha)} \quad (36)$$

where

$$\ln\eta=\frac{\left[Y+\left(\alpha-1\right)p_0\right]}{\left(\alpha-1\right)M}\left[1-\frac{kv(\beta+1)}{1-v\left(2-k\right)}+k\beta\left(1+v-kv\right)\right] \quad (37)$$

$$\omega=\frac{(k+1)\left[Y+(\alpha-1)p_0\right]}{kM(\alpha-1)\left[\alpha+1/k+(1-\alpha)(d_2/b_2)^{k+1}\right]}\left[1+k\alpha\beta(1+v-kv)-\frac{kv(\beta+\alpha)}{1-v(2-k)}\right] \tag{38}$$

With the aid of the transformation variable θ in Equation (39),

$$\theta(r_2)=\omega(d_2/r_2)^{k(1-\alpha)} \tag{39}$$

the integration of Equation (36) over [r_2, d_2] leads to:

$$\omega^{-\gamma}\int_{\theta(r_2)}^{\theta(d_2)} e^{\theta}\theta^{\gamma-1}\mathrm{d}\theta=\frac{\eta}{\gamma}\left[\left(\frac{d_{20}}{d_2}\right)^{k\beta+1}-\left(\frac{r_0}{d_2}\right)^{k\beta+1}\right] \tag{40}$$

where $\gamma=(k\beta+1)/\left[k(\alpha-1)\right]$.

Then putting $r_0=a_0$ and $r_2=a_2$, Equation (40) can be solved with the aid of series expansion of e^{θ} (i.e. $e^{\theta}=\sum_{n=1}^{\infty}\theta^n/n!$, $n!$ represents the factorial of n) as:

$$\sum_{n=0}^{\infty}\frac{\omega^n}{n!(n+\gamma)}\left[1-(d_2/a_2)^{k(1-\alpha)(n+\gamma)}\right]=\frac{\eta}{\gamma}\left[\left(\frac{d_{20}}{d_2}\right)^{k\beta+1}-\left(\frac{a_0}{d_2}\right)^{k\beta+1}\right] \tag{41}$$

It is worth noting that the above displacement analysis can be significantly simplified by ignoring the contribution of elastic strain and/or using the small strain definition within the plastic zone. For example, the right-hand side of Equation (34) will become zero under the former assumption (Vrakas & Anagnostou, 2014; Yu & Houlsby, 1995; Yu & Rowe, 1999). However, to avoid possible errors that are accompanied by these simplifications (Vrakas & Anagnostou, 2014), they are not attempted in this study.

Fully plastic unloading analysis

When the surrounding soil enters the fully plastic unlading phase (i.e. $d_2=b_2$), it is found that the stress distribution can be obtained directly by replacing d_2 with b_2 from Equations (26), (27) and (28) as:

$$\sigma_{r2}=\frac{Y}{\alpha-1}-\frac{Y+(\alpha-1)p_0}{\alpha-1}\left(\frac{b_2}{r_2}\right)^{k(1-\alpha)} \tag{42}$$

$$\sigma_{\theta2}=\frac{Y}{\alpha-1}-\frac{\alpha\left[Y+(\alpha-1)p_0\right]}{\alpha-1}\left(\frac{b_2}{r_2}\right)^{k(1-\alpha)} \tag{43}$$

A large-strain displacement solution for a fully plastic soil cylinder/sphere can be obtained by integrating Equation (36) over [a_2, b_2] as:

$$\sum_{n=0}^{\infty}\frac{\left(\omega|_{d_2=b_2}\right)^n}{n!(n+\gamma)}\left[1-\left(\frac{b_2}{a_2}\right)^{k(1-\alpha)(n+\gamma)}\right]=\frac{\eta}{\gamma}\left[\left(\frac{b_0}{b_2}\right)^{k\beta+1}-\left(\frac{a_0}{b_2}\right)^{k\beta+1}\right] \tag{44}$$

For a cavity unloading from an in-situ stress state (also applicable for unloading analysis from a loading-induced elastic stress state), all the necessary information for determining the complete pressure-contraction curve and stress distributions has been given. Results can be readily obtained following a similar procedure given by Yu (1992, 1993) or in a simplified way of that will be detailed in the next section.

Solutions for unloading from a partially/fully plastic state

This section presents solutions for the analysis of a cavity unloading from a partially or fully plastic stress state (namely cases II and III in Figure 1, $p_{20} \geq p_{1\mathrm{elim}}$).

Elastic unloading analysis

Initially, the unloading is purely elastic. Upon elastic unloading, changes in the stress and displacement can be determined by solving Equations (1), (17) and (18), which gives:

$$\Delta\sigma_r = -(p_2 - p_{20})\frac{(b_2/r_2)^{k+1}-1}{(b_2/a_2)^{k+1}-1} \tag{45}$$

$$\Delta\sigma_\theta = (p_2 - p_{20})\frac{(b_2/r_2)^{k+1}/k+1}{(b_2/a_2)^{k+1}-1} \tag{46}$$

$$\Delta u(r_2) = \frac{(p_2 - p_{20})}{Mr_2^k\left(1/a_2^{k+1}-1/b_2^{k+1}\right)}\left\{(1+v-kv)\left[\left(\frac{r_2}{b_2}\right)^{k+1}+\frac{1}{k}\right]+\frac{v}{1-v(2-k)}\left[1-\left(\frac{r_2}{b_2}\right)^{k+1}\right]\right\} \tag{47}$$

Reverse plasticity occurs once the Mohr-Coulomb yield criterion Equation (6) is satisfied. This condition is firstly satisfied at the inner wall when the cavity pressure reaches its elastic limit $p_{2\mathrm{elim}-2}$. Combining Equation (6), (10), (11), (45) and (46), it gives:

$$p_{2\mathrm{elim}-2} = p_{20} - \frac{A_1(\alpha - 1/\alpha)(c_{20}/a_{20})^{\frac{k(\alpha-1)}{\alpha}}\left[(b_2/a_2)^{k+1}-1\right]}{(\alpha+1/k)(b_2/a_2)^{k+1}+1-\alpha} \tag{48}$$

Elastic-plastic unloading analysis

As the cavity pressure p_2 further reduces, a reverse plastic zone forms and spreads outwards from the inner wall of the cavity (i.e. $a_2 \le r_2 \le d_2$). Equations (2) and (3) define that the current stress state in the soil depends on both the residual stresses due to previous loading and the stress changes due to unloading. Hence, for a cavity unloading from a partially plastic state (i.e. case II in Figure 1), the solution needs to be discussed according to the relative size of the loading-induced plastic zone and the reverse plastic zone as illustrated in Figure 2. The elastic-plastic unloading behaviour of a cavity unloading from a fully plastic state (i.e. case III in Figure 1) is studied simultaneously as follows.

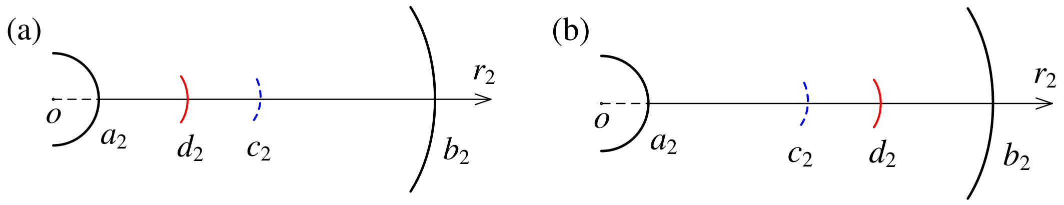

(a) Phase with $d_2 < c_2 \le b_2$ (b) Phase with $c_2 \le d_2 < b_2$

Figure2. Distribution of stress states

Unloading Phase with $d_2 < c_2 \le b_2$

(1) Stress analysis

The unloading-induced changes of the principal stresses in the elastic unloading zone (i.e. $d_2 \le r_2 \le b_2$, Figure 2a) can be determined by solving Equations (1), (17) and (18) as:

$$\Delta\sigma_r = B_{2-2}\left[(b_2/r_2)^{k+1} - 1\right] \tag{49}$$

$$\Delta\sigma_\theta = -B_{2-2}\left[(b_2/r_2)^{k+1}/k + 1\right] \tag{50}$$

In the reverse plastic zone ($a_2 \le r_2 \le d_2$), the principal stresses are determined by jointly solving Equations (1) and (6) as:

$$\sigma_{r2} = Y/(\alpha - 1) + A_{2-2}(d_2/r_2)^{k(1-\alpha)} \tag{51}$$

$$\sigma_{\theta 2} = Y/(\alpha - 1) + A_{2-2}\alpha(d_2/r_2)^{k(1-\alpha)} \tag{52}$$

The constants B_{2-2} and A_{2-2} of integration can be determined based on the continuity condition of stress components at the outer radius of the reverse plastic interface (i.e. at $r_2 = d_2$) as:

$$B_{2-2}=\frac{A_1(\alpha-1/\alpha)(c_{20}/d_{20})^{\frac{k(\alpha-1)}{\alpha}}}{(\alpha+1/k)(b_2/d_2)^{k+1}+1-\alpha} \qquad \text{(while } d_2<c_2\le b_2\text{)} \tag{53}$$

$$A_{2-2}=B_{2-2}\left[(b_2/d_2)^{k+1}-1\right]-A_1(c_{20}/d_{20})^{\frac{k(\alpha-1)}{\alpha}} \qquad \text{(while } d_2<c_2\le b_2\text{)} \tag{54}$$

(2) Displacement analysis

In the elastic unloading zone ($d_2 \le r_2 \le b_2$), the radial displacement can be obtained by integrating Equations (17) and (18) with inputs of Equations (49) and (50) as:

$$\Delta u(r_2)=\frac{-B_{2-2}r_2}{M}\left\{1+v-kv-\frac{v}{1-v(2-k)}+\left[\frac{v}{1-v(2-k)}+\frac{1+v-kv}{k}\right]\left(\frac{b_2}{r_2}\right)^{k+1}\right\} \tag{55}$$

The below relationship between strain and stress is established with reference to the state at the completion of unloading, taking a procedure akin to that of obtaining Equation (34).

$$\Delta\varepsilon_r+k\beta\Delta\varepsilon_\theta=\frac{1}{M}\left\{\left(1-\frac{k\beta v}{1-v(2-k)}\right)\Delta\sigma_r+\left(k\beta(1+v-kv)-\frac{kv}{1-v(2-k)}\right)\Delta\sigma_\theta\right\} \tag{56}$$

According to the definition of logarithmic strains, $\Delta\varepsilon_r$ and $\Delta\varepsilon_\theta$ are expressed as:

$$\Delta\varepsilon_r=\ln(\mathrm{d}r_2/\mathrm{d}r_{20}), \quad \Delta\varepsilon_\theta=\ln(r_2/r_{20}) \tag{57 a,b}$$

Substituting Equations (57 a,b) into Equation (56) gives:

$$\ln\left(r_2^{k\beta}\mathrm{d}r_2/r_{20}{}^{k\beta}\mathrm{d}r_{20}\right)=-\omega_1(d_2/r_2)^{k(1-\alpha)}+\lambda_1(c_{20}/r_{20})^{\frac{k(\alpha-1)}{\alpha}} \tag{58}$$

in which

$$\omega_1=-\frac{A_{2-2}}{M}\left\{1-\frac{k\beta v}{1-v(2-k)}+\alpha\left[k\beta(1+v-kv)-\frac{kv}{1-v(2-k)}\right]\right\} \tag{59}$$

$$\lambda_1=\frac{A_1}{M}\left\{1-\frac{k\beta v}{1-v(2-k)}+\frac{1}{\alpha}\left[k\beta(1+v-kv)-\frac{kv}{1-v(2-k)}\right]\right\} \tag{60}$$

In this case, two transformation variables are introduced, namely:

$$\bar{\theta}(r_2)=\omega_1(d_2/r_2)^{k(1-\alpha)} \quad \square \quad \rho(r_{20})=\lambda_1(c_{20}/r_{20})^{\frac{k(\alpha-1)}{\alpha}} \tag{61 a,b}$$

Then integrating Equation (58) over the interval [r_2, d_2] leads to:

$$d_2^{k\beta+1}\int_{\bar{\theta}(r_2)}^{\bar{\theta}(d_2)} e^{\bar{\theta}}\bar{\theta}^{\gamma-1}\omega_1^{-\gamma}\mathrm{d}\bar{\theta}+\alpha c_1^{k\beta+1}\int_{\rho(r_{20})}^{\rho(d_{20})} e^{\rho}\lambda_1^{\alpha\gamma}\rho^{-\alpha\gamma-1}\mathrm{d}\rho=0 \tag{62}$$

Placing $r_{20}=a_{20}$ and $r_2=a_2$, Equation (62) can be solved with the aid of infinite series as:

$$\sum_{n=0}^{\infty}\frac{d_2^{k\beta+1}\omega_1^{\,n}}{(n+\gamma)n!}\left[1-\left(d_2/a_2\right)^{k(1-\alpha)(n+\gamma)}\right]+\sum_{n=0}^{\infty}\Omega_n^1=0 \tag{63}$$

where

$$\Omega_n^1=\begin{cases}\dfrac{\alpha c_{20}^{k\beta+1}\lambda_1^{\,n}}{n!}\dfrac{k(\alpha-1)}{\alpha}\ln\dfrac{a_{20}}{d_{20}} & \text{, if } n=\alpha\gamma\\ \dfrac{\alpha c_{20}^{k\beta+1}\lambda_1^{\,n}}{(n-\alpha\gamma)n!}\left[\left(c_{20}/d_{20}\right)^{\frac{k(\alpha-1)(n-\alpha\gamma)}{\alpha}}-\left(c_{20}/a_{20}\right)^{\frac{k(\alpha-1)(n-\alpha\gamma)}{\alpha}}\right] & \text{, otherwise}\end{cases} \tag{64}$$

While taking $b_0 \propto \infty$, the above solution reduces to the large-strain solution of Yu and Houlsby (1995) for the cavity contraction analysis in an infinitely large soil mass.

Note that the above solution can also be applied in the analysis of a cavity unloading from a fully plastic stress state before it reaches the reverse fully plastic phase because the condition of $d_2<c_2$ is always fulfilled in this case. However, care should be exercised in the calculation of the residual stress field in the soil as it is different between the partially plastic expansion state and the fully plastic expansion state.

Unloading Phase with $c_2\le d_2<b_2$

(1) Stress analysis

The unloading phase of $c_2\le d_2<b_2$ (Figure 2b) is likely to occur in a lightly pre-loaded soil mass. In this phase, the stress solutions of Equations (49) and (50) for the elastic unloading zone (i.e. $d_2\le r_2\le b_2$) and Equation (51) and (52) for the reverse plastic zone ($a_2\le r_2\le d_2$) are still valid. However, the constants of integration $B_{2\text{-}2}$ and $A_{2\text{-}2}$ need to be replaced by $B_{2\text{-}3}$ and $A_{2\text{-}3}$ below respectively as the stress conditions at $r_2=d_2$ changed.

$$B_{2-3}=\frac{Y+(\alpha-1)p_0+B_1\left[(\alpha+1/k)\left(b_{20}/d_{20}\right)^{k+1}+1-\alpha\right]}{(\alpha+1/k)\left(b_2/d_2\right)^{k+1}+1-\alpha}\quad(\text{while } c_2\le d_2<b_2) \tag{65}$$

$$A_{2-3}=-\frac{Y+(\alpha-1)p_0}{(\alpha-1)}-B_1\left[\left(\frac{b_{20}}{d_{20}}\right)^{k+1}-1\right]+B_{2-3}\left[\left(\frac{b_2}{d_2}\right)^{k+1}-1\right]\quad(\text{while } c_2\le d_2<b_2) \tag{66}$$

Then according to Equation (2) and (3) (i.e. $\Delta\sigma_r=\sigma_{r2}-\sigma_{r20}$ and $\Delta\sigma_\theta=\sigma_{\theta2}-\sigma_{\theta20}$), the changes in stress due to unloading can be readily determined using Equation (10), (11), (51), (52), (65) and (66) for the zone $a_2 \le r_2 \le c_2$ (named as loading plastic and reverse plastic zone) and Equations (12), (13), (51), (52), (65) and (66) for the zone $c_2 \le r_2 \le d_2$ (named as loading elastic and reverse plastic zone), respectively.

(2) Displacement analysis

In this unloading phase, the radial displacement in the elastic zone (i.e. $d_2 \le r_2 \le b_2$) can be calculated by Equation (55) with the value of $B_{2\text{-}3}$ of Equation (65).

In the reverse plastic zone $a_2 \le r_2 \le d_2$ (Figure 2b), a large-strain displacement analysis can be carried out following the same procedure of deriving Equations (31)-(64). However, due to the difference in the residual stress field between the zone of $a_2 \le r_2 \le c_2$ and the zone of $c_2 \le r_2 \le d_2$, the distribution of displacement in the soil now needs to be derived by considering these two zones separately, which is continuous at the interface $r_2 = c_2$.

In the loading-elastic and reverse plastic zone of $c_2 \le r_2 \le d_2$, substituting Equations (12), (13), (51), (52), (57 a,b), (65) and (66) into Equation (56) leads to:

$$\ln\left(r_2^{k\beta}\mathrm{d}r_2 / r_{20}^{k\beta}\mathrm{d}r_{20}\right) = \ln\eta_1 - \omega_2\left(d_2/r_2\right)^{k(1-\alpha)} + \lambda_2\left(b_{20}/r_{20}\right)^{k+1} \tag{67}$$

where

$$\ln\eta_1 = \frac{1}{M}\left[1 - \frac{k\beta v}{1-v(2-k)} + k\beta(1+v-kv) - \frac{kv}{1-v(2-k)}\right]\left(p_0 + \frac{Y}{\alpha-1} - B_1\right) \tag{68}$$

$$\lambda_2 = \frac{B_1}{M}\left[1 - \frac{k\beta v}{1-v(2-k)} - \beta(1+v-kv) + \frac{v}{1-v(2-k)}\right] \tag{69}$$

$$\omega_2 = -\frac{A_{2-3}}{M}\left\{1 - \frac{k\beta v}{1-v(2-k)} + \alpha\left[k\beta(1+v-kv) - \frac{kv}{1-v(2-k)}\right]\right\} \tag{70}$$

Then the integration of Equation (67) in the interval of $[c_2, d_2]$ gives:

$$\frac{1+k}{k(\alpha-1)}\sum_{n=0}^{\infty}\frac{d_2^{k\beta+1}\omega_2^{\,n}}{(n+\gamma)n!}\left[1-\left(d_2/c_2\right)^{k(1-\alpha)(n+\gamma)}\right] + \sum_{n=0}^{\infty}\Omega_n^2 = 0 \tag{71}$$

where

$$\Omega_n^2 = \begin{cases} \dfrac{\eta_1 b_{20}^{k\beta+1}\lambda_2^{\,n}(k+1)}{n!}\ln\dfrac{c_{20}}{d_{20}} & \text{, if } n = \dfrac{k\beta+1}{k+1} \\ \dfrac{\eta_1 b_{20}^{k\beta+1}\lambda_2^{\,n}}{\left(n-\dfrac{k\beta+1}{k+1}\right)n!}\left[\left(b_{20}/d_{20}\right)^{\left(n-\frac{k\beta+1}{k+1}\right)(k+1)} - \left(b_{20}/c_{20}\right)^{\left(n-\frac{k\beta+1}{k+1}\right)(k+1)}\right] & \text{, otherwise} \end{cases} \tag{72}$$

In the loading-plastic and reverse plastic zone of $a_2 \le r_2 \le c_2$, the displacement at $r_2 = a_2$ can be obtained by integrating Equation (67) in the interval of [a_2, c_2], which is:

$$\sum_{n=0}^{\infty} \frac{d_2^{k\beta+1}\omega_2^{\,n}}{(n+\gamma)n!}\left[\left(d_2/c_2\right)^{k(1-\alpha)(n+\gamma)} - \left(d_2/a_2\right)^{k(1-\alpha)(n+\gamma)}\right] + \sum_{n=0}^{\infty}\Omega_n^3 = 0 \tag{73}$$

where

$$\Omega_n^3 = \begin{cases} \dfrac{\alpha c_{20}^{k\beta+1}\lambda_1^{\,n}}{n!}\dfrac{k(\alpha-1)}{\alpha}\ln\dfrac{a_{20}}{c_{20}} & \text{, if } n = \alpha\gamma \\ \dfrac{\alpha c_{20}^{k\beta+1}\lambda_1^{\,n}}{(n-\alpha\gamma)n!}\left[1-\left(c_{20}/a_{20}\right)^{\frac{k(\alpha-1)(n-\alpha\gamma)}{\alpha}}\right] & \text{, otherwise} \end{cases} \tag{74}$$

Reverse fully plastic unloading analysis

With sufficiently large contraction, the cylinder/sphere of soil will enter a fully plastic unloading phase. This may be reached from either a partially plastic state (i.e. case II in Figure 1) or a fully plastic state (i.e. case III in Figure 1) as studied separately below.

Reverse fully plastic unloading of Case II

This state follows the unloading phase of $c_2 \le d_2 < b_2$ that was studied previously. The stress solution of Equations (51) and (52) still holds in this phase, but A_{2-2} and d_2 therein need to be replaced by A_{2-4} and b_2, respectively. The new integration constant A_{2-4} is determined according to the given stress boundary conditions in Equation (5 a,b) as:

$$A_{2-4} = -\left[p_0 + Y/(\alpha-1)\right] \qquad (\text{while } c_2 < d_2 = b_2) \tag{75}$$

The distribution of displacement in the soil can be obtained with the same procedure of deriving Equations (67)-(74), considering the zone $a_2 \le r_2 \le c_2$ and the zone of $c_2 \le r_2 \le b_2$ separately. Similarly, it is found that the displacement solution can be obtained by replacing A_{2-4} and d_2 with A_{2-4} and b_2, respectively, in Equation (67)-(74).

Reverse fully plastic unloading of Case III

This is for the fully plastic unloading analysis of the case that the soil cylinder/sphere was previously loaded to be fully plastic ($c_2 = b_2$). In this case, the stress distribution in the soil can be obtained by Equation (51) and (52), replacing d_2 and A_{2-2} with b_2 and the new constant A_{2-5} (i.e. Equation (76)), respectively.

$$A_{2-5} = A_{2-4} = -\left[p_0 + Y/(\alpha - 1) \right] \qquad (\text{while } c_2 = d_2 = b_2) \tag{76}$$

The large-strain displacement of the surrounding soil during this fully plastic unloading phase can be described by Equations (55), (56), (59) and (60) as well while replacing d_2, c_1, and A_{2-2} therein with b_2, b_2 and A_{2-5}, respectively.

Solution procedure

All the necessary information for determining the pressure-contraction curve and stress distributions has been given. As the pressure-expansion relationship is not expressed in terms of a single equation, it is instructive to summarize the procedure that can be used to construct the complete pressure-contraction curve as below:

(1) Choose input soil parameters: E, v, c, φ, ψ; in-situ stress: p_0; cavity geometry information: k, b_0 and a_0; and the reference state parameter: a_{20};

(2) Calculate the derived parameters G, Y, α, β, γ, M and the reverse limit $p_{2\text{elim}-2}$ (Equation (48));

(3) Calculate the pressure-expansion curve in the loading process until the inner cavity radii reaches a_{20}, and then record c_{20}, b_{20}, and p_{20} for elastic-plastic loading process, or b_{20} and p_{20} for fully plastic loading process. The solution procedure is available in Yu (1992, 1993);

(4) Calculate A_1 and B_1 from Equations (14) and (15), respectively, with the known value of c_{20} and b_{20}. The stress field at the end of loading process (σ_{r20} and $\Delta\sigma_{\theta 20}$) can be obtained from Equations (10) and (11) for the plastic zone and Equations (12) and (13) for the elastic zone;

(5) For elastic unloading analysis, choose a pressure p_2 (p_{20}<p_2< $p_{2\text{elim}-2}$) and calculate $\Delta\sigma_r$ and $\Delta\sigma_\theta$ from Equations (45) and (46), respectively. Then the distribution of stress can be obtained from Equations (2), (3) and (10)-(13). And the relative displacement Δu could be calculated from Equation (47);

(6) If p_2< $p_{2\text{elim}-2}$, elastic-plastic (a_{20}<c_{20}<b_{20}) or fully plastic (c_{20}=b_{20}) unloading analysis is needed;

(7) In the case of a_{20}<c_{20}<b_{20} (Case II in Figure 1):

(a) while $d_2 < c_2 \le b_2$, choose a value of d_{20} ($a_{20}<d_{20}<c_{20}$), calculate d_2 and b_2 from Equation (55) with the known value of d_{20} and b_{20}; then calculate a_2 from Equations (63) and (64) with the known values of d_2, d_{20}, b_2 and c_{20}, and p_2 from Equations (51) and (54).

When d_{20}, d_2, b_2 are known, $B_{2\text{-}2}$ and $A_{2\text{-}2}$ can be calculated from Equations (53) and (54), and then the distribution of stress can also be derived from Equations (49)-(52).

(b) while $c_2 \le d_2 < b_2$, choose a value of d_{20} ($c_{20}<d_{20}<b_{20}$), calculate d_2 and b_2 from Equation (55) with the known value of d_{20} and b_{20}; calculate c_2 from Equations (71) and (72) with the known values of d_2, d_{20}, b_2 and c_{20}; calculate a_2 from Equations (73) and (74); then calculate p_2 from Equation (51) by setting $r_2=a_2$. Note that in all calculations of this phase, $A_{2\text{-}2}$ and $B_{2\text{-}2}$ need to be replaced by $A_{2\text{-}3}$ and $B_{2\text{-}3}$ (Equations (65) and (66)), respectively;

With the values of $A_{2\text{-}3}$, $B_{2\text{-}3}$, b_2 and d_2, the distribution of stress components can be calculated from Equations (49)-(52) by replacing $A_{2\text{-}2}$ and $B_{2\text{-}2}$ with $A_{2\text{-}3}$ and $B_{2\text{-}3}$, respectively.

(c) while $d_2=b_2$, choose a value of b_2/c_2 (greater than b_{20}/c_{20}), calculate c_2 and b_2 from Equations (71) and (72); calculate a_2 from Equations (73) and (74) with the known values of b_2 and c_2; then calculate p_2 from Equation (51) with $r_2=a_2$. In this phase, $A_{2\text{-}2}$ in the relevant equations needs to be replaced by $A_{2\text{-}4}$ (Equation (75)), and the stress components can be obtained from Equations (51) and (52).

(d) For the case of $c_{20}<b_{20}$, repetition of steps of (a) and (b) for varying d_{20}, and (c) for varying b_2/c_2 provides the data for a complete pressure-contraction curve.

(8) In the case of $c_{20}=b_{20}$ (Case III in Figure 1):

(e) while $d_2< c_2=b_2$, step (a) still holds;

(f) while $c_2= d_2= b_2$, choose a value of b_2/c_2 (greater than the value of b_2/c_2 in the previous step), calculate b_2 and a_2 from Equations (63) and (64); then calculate p_2 from Equation (51) with $r_2=a_2$. In this phase, $A_{2\text{-}2}$ in the relevant equations needs to be replaced by $A_{2\text{-}5}$ (Equation (76)). Similarly, the distribution of stress components can be obtained from Equations (51) and (52) by replacing $A_{2\text{-}2}$ by $A_{2\text{-}5}$.

Repetition of steps of (e) for varying d_{20} and (f) for varying of b_2/a_2 provides the data for complete pressure-contraction curve. Note that, for the cases in a frictionless soil, results can be calculated with the above solutions using very small φ values.

Solution validation and result analysis

Unloading curves from an in-situ stress state

At first, the unloading solution from an in-situ stress state is validated by comparing with the solution of Vrakas and Anagnostou (2014) in the special case of a cavity in an infinite soil mass. Taking the material parameters: p_0=22.5MPa, E=2000MPa, c=0.25MPa, φ=23°, ψ=3° and ν=0.25 that were used by Vrakas and Anagnostou (2014), both the pressure-contraction curve and the distribution of stresses and the radial displacement at the moment of p_2=0MPa were calculated, and they are compared with those obtained by Vrakas and Anagnostou (2014) in Figure 3. The comparisons in Figure 3 indicate that their solution can be recovered by the present solution assuming $b_0 / a_0 \propto \infty$, neglecting the out-of-plane plastic flow effect which proved to be insignificant (Reed, 1986; Vrakas & Anagnostou, 2014).

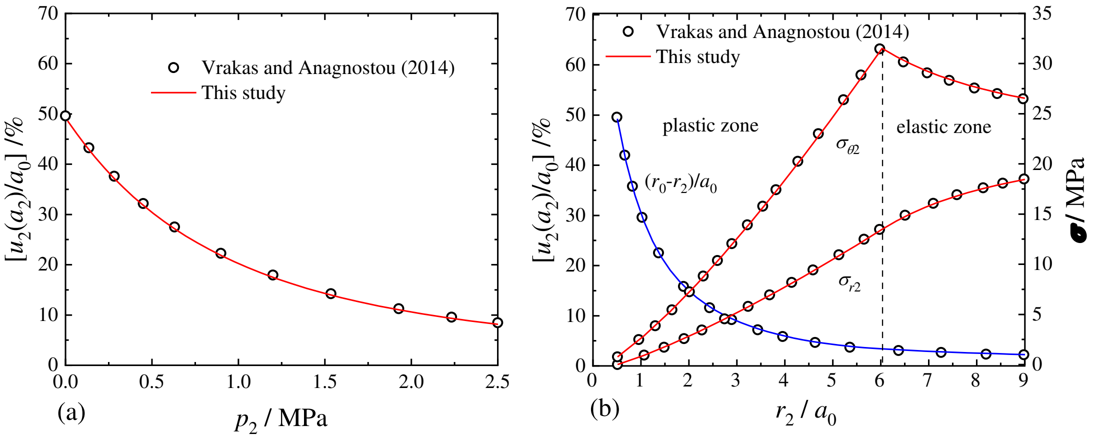

(a) pressure-contraction curve. (b) distribution of stresses and radial displacement.

Figure3. A cylindrical cavity unloading from an in-situ stress state (Sedrun section of the Gotthard Base Tunnel (Vrakas & Anagnostou, 2014))

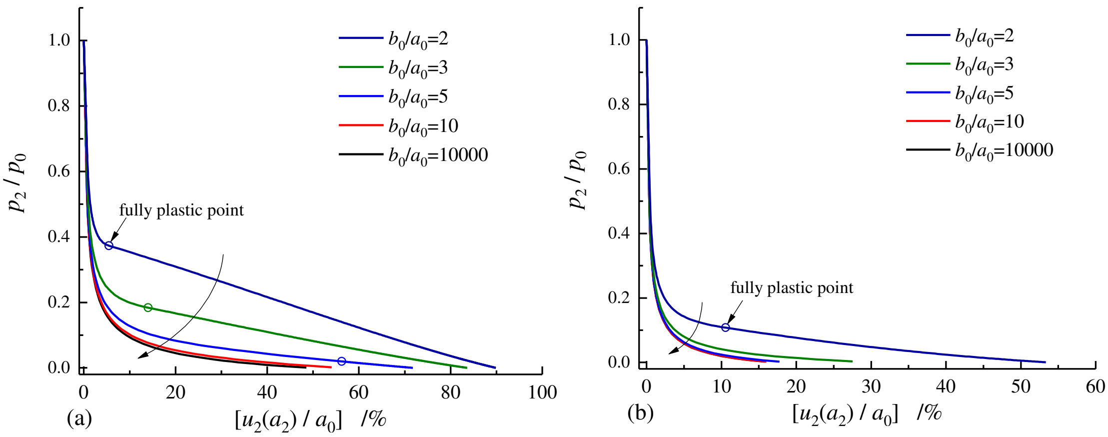

(a) cylinders (b) spheres

Figure4. Pressure-contraction curves with varying b_0/a_0

To indicate the effects of the cavity geometry ratio b_0/a_0, example cavity pressure-contraction curves with different values of b_0/a_0 are computed using the same material parameters as above. The results in Figure 4 show that the value of b_0/a_0 greatly influences the cavity unloading behaviour when it is smaller than a limit value for both hollow cylinders and spheres. The value of this limit ratio varies with soil properties and is generally smaller for a hollow sphere than a cylinder. With the same level of contraction (e.g. $(a_{20}-a_0)/a_0$), the magnitude of unloading (e.g. $(p_{20}-p_0)/p_0$) is smaller for a thinner cylinder/sphere of soil while b_0/a_0 is smaller than the limit ratio. In other words, with the same magnitude of unloading, greater radial contraction may occur for a thinner hollow cylinder/sphere. Tunneling involves the removal of soil/rock masses from their initial locations, and this is analogy to the problem of cavity unloading from an in-situ stress state (Mair & Taylor, 1993; Mo & Yu, 2017; Ogawa & Lo, 1987; Vrakas & Anagnostou, 2014; Yu & Rowe, 1999). Experimental results (e.g. (Franza et al., 2019)) have shown that the ground response curves (GRCs) of shallow tunnels in sands vary with the tunnel depth ratio (e.g. soil cover depth/tunnel radius) in a very similar fashion as that is shown in Figure 4.

Apart from the geometry ratio b_0/a_0, soil strength and stiffness parameters also affect the cavity unloading behaviour. Their influences are akin to those observed in unloading analyses of a cavity in an infinite soil mass, which can refer to the results of Yu and Rowe (1999) and Vrakas and Anagnostou (2014).

Unloading curves from a partially/fully plastic state

Using the same soil model, Yu and Houlsby (1995) developed an analytical large-strain solution for unloading analysis of an infinite soil mass under a loading-induced partially plastic state. The paper extended their solution to the more general case of a hollow cylinder/sphere of soil. For validation, results obtained by these two solutions are compared in Figure 5. It is shown that the present solution can exactly recover to their solution, taking $b_0 / a_0 \propto \infty$. Note that the solutions of Yu (1992, 1993) were used to calculate the expansion curves and the reference stress state in the validation and following analyses.

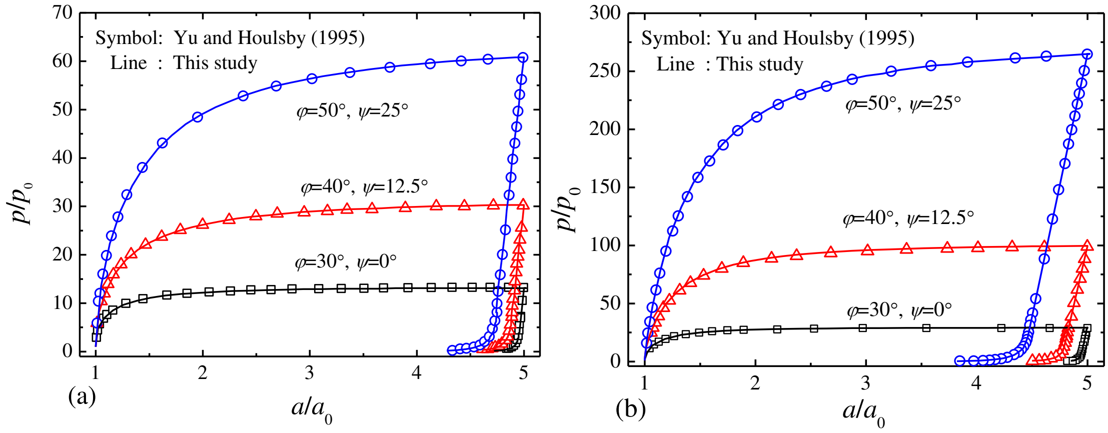

(a) cylindrical cavities (b) spherical cavities

Figure5. Comparison with results of Yu and Houlsby (1995) (E/p_0=1300, v=0.3 and c=0).

To show the effects of the reference stress state on the unloading behaviour of a finite soil mass, a selection of results of loading and unloading curves with different magnitudes of preloading and values of b_0/a_0 are presented in Figures 6-9. The soil parameters of φ=40°, ψ=20°, v=0.3, c=0 and E/p_0=1300 were used. In Figures 6 and 7, two typical ratios of the initial outer to inner radii of a finite soil mass are considered (e.g. b_0/a_0=10000 or b_0/a_0=5), and the unloading is assumed to start after different magnitudes of expansion (i.e. a_{20}/a_0). In Figures 8 and 9, loading and unloading curves with different values of b_0/a_0 are plotted, in which the applied cavity pressure is removed when the expansion ratio a_{20}/a_0 is equal to 3 and 1.15, respectively. In the figures, the triangle represents the point when the elastic-plastic interface reaches the outer boundary of the hollow cylinder/sphere during loading (i.e. $c_1=b_1$); the circle for each curve represents the point when plastic unloading occurs (i.e. $d_2=a_2$).

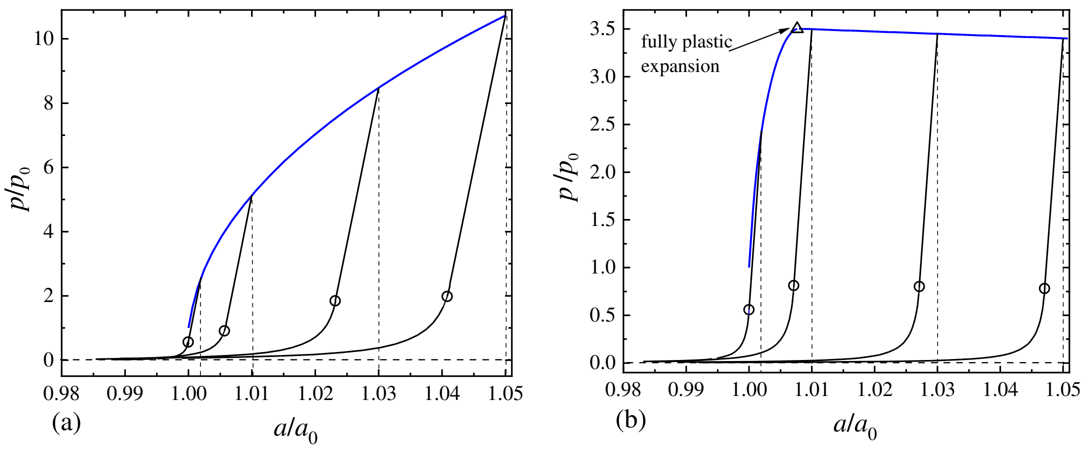

(a) b_0/a_0=10000 (b) b_0/a_0=5

Figure6. Unloading curves of soil cylinders from varying reference stress states

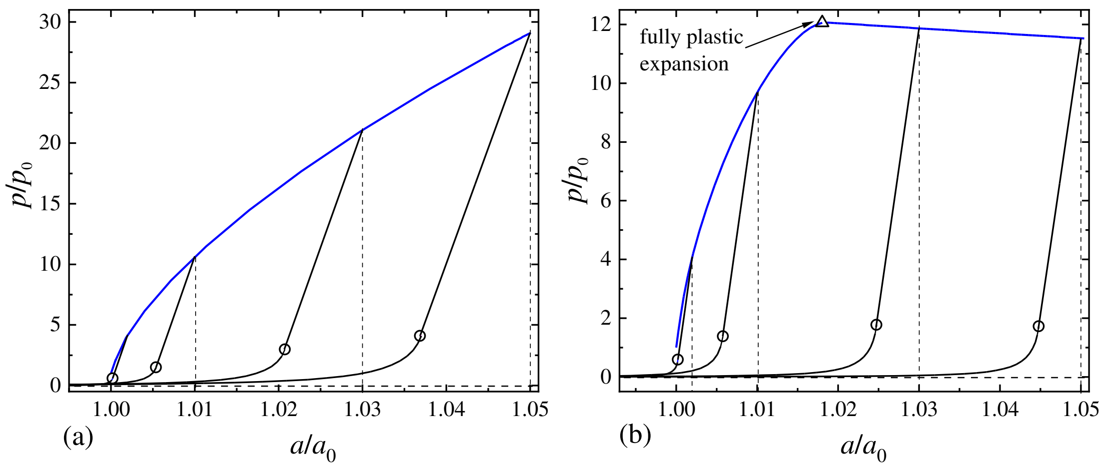

(a) b_0/a_0=10000 (b) b_0/a_0=5

Figure7. Unloading curves of soil spheres from varying reference stress states

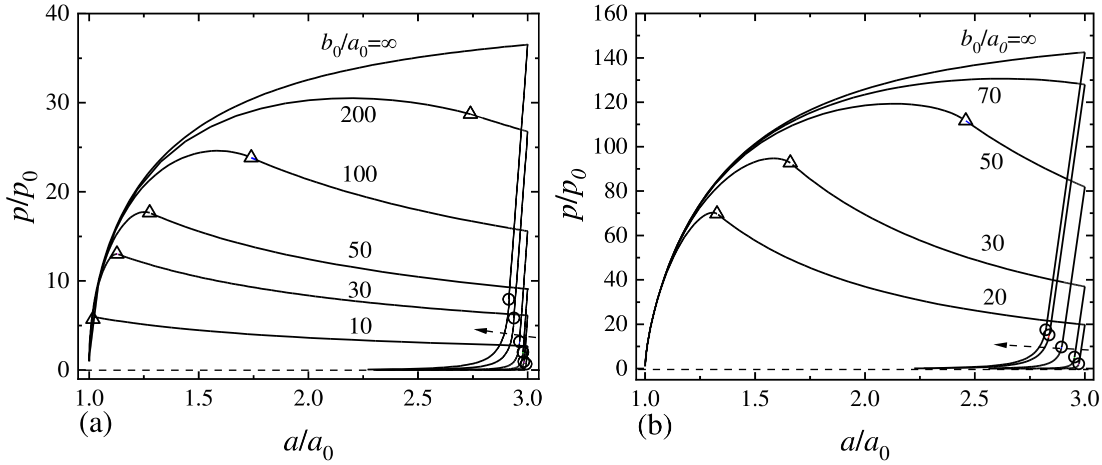

(a) cylinders (b) spheres

Figure8. Variation of loading and unloading curves with b_0/a_0 (a_{20}/a_0=3)

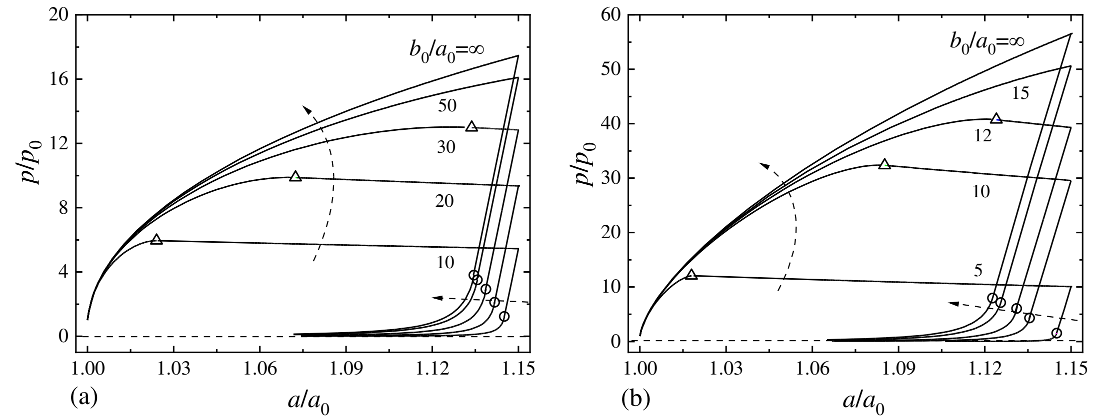

(a) cylinders (b) spheres

Figure9. Variation of loading and unloading curves with b_0/a_0 (a_{20}/a_0=1.15)

Figures 6-9 show that initially the internal cavity pressure reduces rapidly with cavity contractions in the elastic unloading phase (i.e. Equations (45)-(47)). The unloading curves in the non-dimensional plot of p_2/p_0 against a_2/a_0 are almost linear and parallel with each other in this phase. Although the slope of the unloading curve is insensitive to the initial geometry ratio b_0/a_0 and the previous loading history (e.g. a_{20}/a_0), these factors affect the maximum amount of the stress reduction during elastic unloading. Due to the residual stresses generated during previous loading (i.e. the so-called 'overstrain' effect (Hill, 1950; Zhao & Wang, 2010)), the elastic unloading process is much longer than the initial elastic loading process.

The above intrinsic characteristics of the elastic unloading process have been used in various applications such as the control of unloading-reloading loops of pressuremeter tests and the shakedown analysis. As pointed out by Wroth (1982), the soil stiffness can be obtained from the unloading-reloading loop of self-boring pressuremeter tests. While conducting unloading-reloading loops, it is important to ensure that the loop deformation remains in an elastic state. For a linear elastic-perfectly plastic Mohr-Coulomb material, Equations (10) and (48) can be used to determine the maximum reduction of the effective pressure allowed for elastic unloading in pressuremeter tests. In an infinite soil mass, the maximum cavity pressure reduction is a function of soil strength parameters (e.g. friction angle and cohesion) and the loading-induced stress state (e.g. p_{20}) (Wroth, 1982; Zhao & Wang, 2010). However, it also varies with the value of b_0/a_0 for the unloading of a finite soil mass (e.g. Figures 6(b), 7(b), 8 and 9). An example application to the shakedown analysis will be given in the next section.

Once the cavity pressure reduces to be smaller than the elastic limit (i.e. Equation (48)), the unloading curve becomes highly non-linear as reverse yielding occurs in the soil. The radial convergence accelerates as the plastic region spreads out with smaller internal confining pressure. When the cavity pressure reaches a sufficiently low value, the radial convergence increases sharply until the inner cavity is filled. In general, the speed of transition from a purely elastic state to the steady or limit state during unloading is much faster than that occurred in the initial loading process, and it varies with the cavity shape (normally, it is faster for a spherical cavity than a cylindrical cavity). The minimum internal pressure that the soil can sustain mainly depends on the soil strength parameters as defined in Equation (51), for example, it is close to zero for cohesionless soils but could be negative for cohesive soils or rocks. Figures 6-9 show that this limit value of unloading pressure does not significantly vary with the value of b_0/a_0 and the loading history.

As mentioned previously, experimental studies on both self-boring and full-displacement pressuremeters (Hughes & Robertson, 1985; Schnaid & Houlsby, 1992) have shown the unloading portion of pressuremeter curves is less sensitive to initial soil disturbance than the loading portion. This is consistently observed in the results of Figures 6-9. Besides, the results indicate that the shape of the unloading curve is also less sensitive to the geometry ratio b_0/a_0 than the loading curve in a finite soil mass. This suggests that the use of the unloading curve of pressuremeter tests to measure the soil properties may also help to remove the boundary effects that are commonly encountered in small-sized calibration chambers.

Example geotechnical applications

Thickness of frozen cylinder earth walls

Artificial ground freezing has been widely used to stabilize temporarily the ground in order to provide ground support and/or exclude groundwater from an excavation until the final retaining and lining structures are constructed (Andersland & Ladanyi, 2004; Sanger & Sayles, 1979; Viggiani & Casini, 2015; Zhang et al., 2018). From a structural point of view, determination of the geometry and the thickness of a frozen wall is one of the main concerns for practitioners. Because of the relatively high compressive and low tensile strengths of frozen soil, curved arch walls, particularly circular walls, are often selected with priority. The unloading model of a cylinder unloading from an in-situ stress state that was studied previously has been commonly used to determine the thickness of a circular frozen wall (Andersland & Ladanyi, 2004; Klein & Gerthold, 1979; Sanger & Sayles, 1979). For example, assuming $\sigma_{r2}\big|_{r_2=b_2}=-p_0$ and $\sigma_{r2}\big|_{r_2=a_2}=0$ (i.e. no internal support), Sanger and Sayles (1979) proposed Equation (77) to estimate the minimum thickness of a cylinder wall. Klein and Gerthold (1979) extended this solution to the case where the internal pressure acting on the wall equals p_2 (i.e. $\sigma_{r2}\big|_{r_2=a_2}=-p_2$), thereby Equation (78) was given. These solutions were obtained by solving the equilibrium equation (1) and the Mohr-Coulomb yield function (6). Therefore, they can be recovered by Equation (26) or (30) considering the boundary conditions they adopted.

$$\left(b_0/a_0\right)^{\alpha-1}=\frac{p_0+c\cot\varphi}{c\cot\varphi} \tag{77}$$

$$\left(b_0/a_0\right)^{\alpha-1}=\frac{p_0+c\cot\varphi}{p_2+c\cot\varphi} \tag{78}$$

In both Equations (77) and (78), a hidden assumption is that the cylinder wall of frozen soil becomes unstable once it becomes fully plastic. This is a typical large deformation problem, and displacements of the cavity during elastic-plastic contractions can be calculated by using Equations (30), (32a, b) and (44). Adopting the criterion of Sanger and Sayles (1979) (i.e. $p_{2\text{fp}-\lim}=0$ in Equation (30)), new results are calculated considering the large deformation effects with typical soil properties of v=0.3, E/p_0=100 and ψ=min(0, φ-20). The new results are compared with the published results of Sanger and Sayles (1979) in Figure 10. It is shown that Equation (77) tends to give conservative predictions of the minimum thickness of a cylinder wall due to the lack of accounting for its radial convergence, whose effects become more significant at larger values of the in-situ earth pressure and the friction angle of soil.

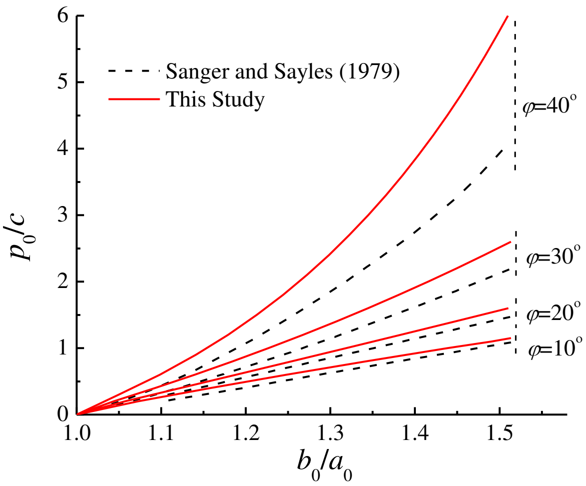

Figure10. Comparison of design charts for circular frozen walls

In addition to the requirement of stability, frozen earth walls may also be designed under displacement control on the basis of required excavation limits and the available space on site (Andersland & Ladanyi, 2004). For example, taking 2% cavity strain (i.e. a_2/a_0=0.98) as the maximum allowable radial convergence of a cylinder wall, the minimum internal pressure required can be obtained by the cylindrical unloading solution from an in-situ state. Example results are presented in Figure 11 with varying strength and stiffness parameters of frozen soils. It is shown that the self-stability of a cylinder wall, in general, increases with the thickness ratio, the frictional strength and stiffness of the soil, thus less internal support is required accordingly.

Adopting different control standards, the application of the large strain in-situ unloading solution to the preliminary structural design of frozen cylinder walls is illustrated in Figures 10 and 11. It needs to be pointed out that the boundary conditions at the outer wall of the cylinder were simplified as a constant radial pressure whose value equals the in-situ stress. In fact, however, the outside confining pressure may reduce with contractions of the cylinder. Thus, this method still tends to be conservative as well. Additionally, it should bear in mind that the above analyses focused on the short-term unloading behaviour. For the long-term stability and deformation analysis, the time-dependent behaviour of frozen soils (e.g. creep strength) needs to be taken into account (Andersland & Ladanyi, 2004; Sanger & Sayles, 1979).

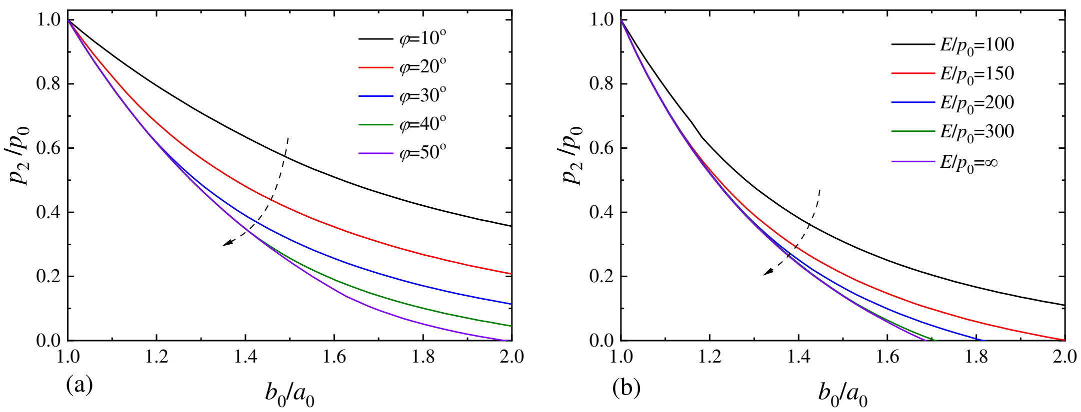

(a) variation with angle of friction (E/p_0=100) (b) variation with stiffness (φ=30°)

Figure11. Internal cavity pressure at a radial displacement of 2% (v=0.3 and c/p_0=0.3)

Prediction of pressuremeter curves

Based on the analogy between pressuremeter tests and a long cylindrical cavity upon loading and unloading, cavity expansion and contraction solutions have been used in the interpretation of pressuremeter tests with considerable success (Clarke, 1995; Mair & Wood, 1987; Wroth, 1984; Yu, 2000). As summarized by Schnaid et al. (2000), the methods of interpreting pressuremeter tests can be broadly categorised into two groups: in the first group each parameter of soil is assessed independently from one portion of the pressuremeter curve; in the second the whole pressuremeter curve (both loading and unloading portions) is taken into account. Using the closed-form expansion and contraction solutions of Yu and Houlsby (1991,1995), Schnaid et al. (2000) analysed many site pressuremeter tests, from which a set of fundamental parameters of soil can be derived. In modelling site pressuremeter tests, it is reasonable to assume the surrounding soil to be horizontally infinite. However, this might be questionable for the modelling of laboratory pressuremeter tests in small-sized calibration chambers as highlighted previously (Alsiny et al., 1992; Fahey, 1986; Jewell et al., 1980; Juran & BenSaid, 1987; Schnaid & Houlsby, 1991).

To account for the possible boundary effects during cavity expansion, Yu (1992, 1993) extended the solution of Yu and Houlsby (1991) to the case in a finite soil mass. Likewise, an extension of the solution of Yu and Houlsby (1995) was obtained in this paper for the analysis of a cavity in a finite soil mass. Now, using the loading solution of Yu (1992) and the present unloading solution in combination, the method proposed by Schnaid et al. (2000) can be extended for the interpretation of pressuremeter tests performed in calibration chambers of a constant lateral stress boundary (i.e. the BC1-type boundary (Ghionna & Jamiolkowski, 1991)). This is evaluated by comparing with the experimental results of pressuremeter tests obtained by Ajalloeian (1996).

A number of pressuremeter tests were performed by Ajalloeian (1996) in a calibration chamber using dry Stockton Beach sand. The ratio of the chamber diameter (1000mm) to the pressuremeter diameter D (30mm) was 33.3. As the pressuremeter is assumed to be infinitely long in the plane strain cylindrical cavity model, test data obtained with pressuremeters of the longest membrane length L available were selected in the analysis to minimize the possible end effects (Ajalloeian & Yu, 1998; Houlsby & Carter, 1993). In specific, L/D was 15 for the test in the loose sand (test ID: 15LK1P100, relative density D_r=27.5%); L/D was 20 for the tests in the medium dense (test ID: 20MK1P100, D_r=63.3%) and dense sand samples (test ID: 20DK1P100, D_r=86.8%) (see Figure 12).

Based on the loading solution of Yu (1992) and the unloading solution of this study (Equations (45)-(76)), the pressuremeter tests are interpreted following the curve fitting method proposed by Schnaid et al. (2000) as follows:

(a) Initial stress state. The initial mean effective stress was 100kPa and the initial stress ratio of the effective vertical stress to the effective horizontal stress was 1 in the tests (Ajalloeian, 1996). The same initial stress state was used in the modelling.

(b) Shear modulus. For the loading portion, the curve fitting was initiated using the tangent stiffness value of the initial portion of the loading curve (Ajalloeian, 1996); for the unloading portion, the value of the shear modulus was estimated by drawing a single line between the point that defines the end of the loading and the representative point of the theoretical plastic reverse of the experimental unloading curve (Schnaid et al., 2000). The Poisson's ratio was assumed to be 0.3.

(c) Strength parameters. The dilation angle ψ was calculated using the correlation of Rowe (1962) (i.e. Equation (79)). The critical state friction angle φ_{cv} of the Stockton Beach sand required in Equation (79) is 31° (Ajalloeian, 1996). The cohesion was set as zero for the dry sand. Then based on the cavity expansion and contraction solutions and the measured pressuremeter curves (both loading and unloading portions), the plane strain friction angle φ_{ps} was back-calculated using a curve fitting technique.

$$\sin\psi = \frac{\sin\varphi_{ps} - \sin\varphi_{cv}}{1 - \sin\varphi_{ps}\sin\varphi_{cv}} \tag{79}$$

Figure 12 presents the predicted and the measured loading and unloading curves. The comparison shows that a good fit (the correlation coefficient R^2>0.99 in all three cases compared) was achieved between theory and data over the whole curve of loading and unloading. In Figure 13, the back-calculated friction angles are compared with the data from triaxial tests measured by Ajalloeian (1996). The relationship $8\varphi_{ps} = 9\varphi_{tri}$ (Wroth, 1984) was used to convert the triaxial friction angle φ_{tri} and the plane strain friction angle φ_{ps} for comparison. Results obtained by Ajalloeian (1996) using other common theoretical methods (e.g. (Hughes et al., 1977; Manassero, 1989; Yu, 1994)) are also plotted in Figure 13. It is shown that the combined use of the loading solution of Yu (1992) and the present unloading solution from an elastic-plastic state as well as the curve-fitting technique of Schnaid et al. (2000) gave the best estimate of the soil strength parameters in the compared cases. The close agreement between theoretical and experimental results in Figures 12 and 13 indicates that this method is able to construct a theoretical curve that reproduces a pressuremeter test from which fundamental soil parameters can be derived reasonably well.

Note that the maximum cavity strain was less than 11% and a large diameter ratio of the chamber to the pressuremeter was intentionally used in the tests of Ajalloeian (1996) to minimize the boundary effect. Therefore, the difference of the friction angle back-calculated with or without considering the size of the sand sample is not significant in these tests (Figure 13). Much stronger boundary effects may appear in tests performed in smaller sand samples as shown in Figure 9 and observed by Jewell et al. (1980), Fahey (1986), Schnaid and Houlsby (1991) and Alsiny et al. (1992), among others. Under this circumstance, the advantages of the present method will be more obvious.

It is necessary to bear in mind that as an elastic-perfectly plastic soil model was used, the non-linear elastic (e.g. stress and strain-dependent shear modulus) and strain hardening/softening behaviour of sand (e.g. non-constant dilatancy) cannot be realistically modelled by the present solutions (Fahey & Carter, 1993; Manassero, 1989). The constraints imposed by these simplifications may introduce some limits to the quality of the comparisons but enforce the consistency among all parameters (Schnaid et al., 2000).

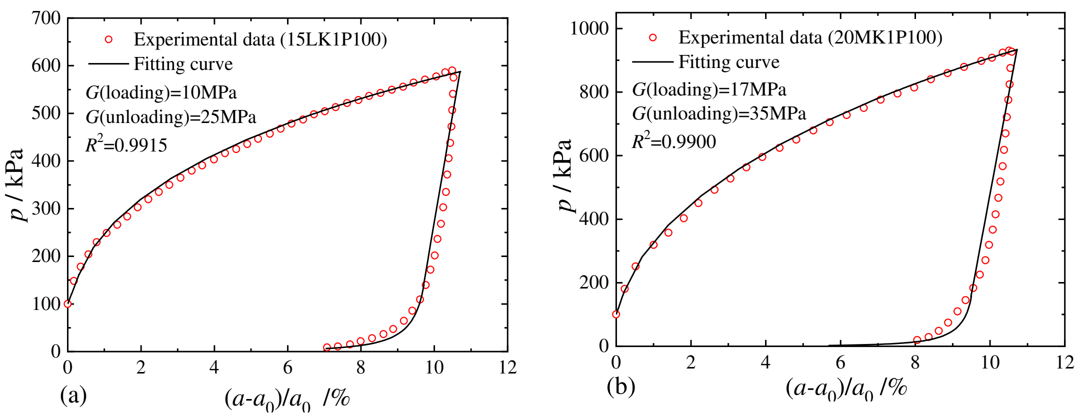

(a) loose sand (b) medium dense sand

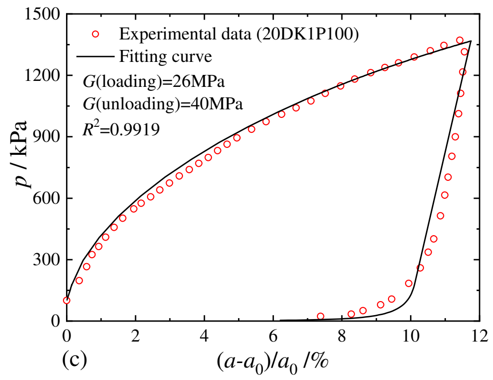

(c) dense sand

Figure12. Comparisons between theoretical and experimental pressuremeter curves (test data from Ajalloeian (1996)).

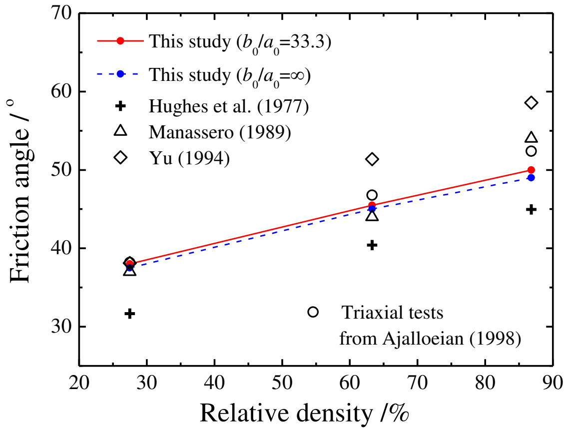

Figure13. Back-calculated and measured plane strain friction angles

Optimal thickness of a hollow cylinder/sphere for overstrain

Several stress limits are of great concern in the stress analysis and optimal design of a hollow cylinder/sphere, for example, the elastic limit, the plastic limit and the shakedown limit (Hill, 1950; Xu & Yu, 2005; Zhao & Wang, 2010). In the process of loading, the elastic limit $p_{1\mathrm{elim}}$ (i.e. while $c_1=a_1$) and plastic limit $p_{1\mathrm{plim}}$ (i.e. while $c_1=b_1$) were given in Equations (9) and (16), respectively. In the subsequent unloading process, reverse yielding occurs at the inner wall of the cavity (i.e. $d_2=a_2$) while the cavity pressure reduces to be equal to $p_{2\mathrm{elim}-2}$ (i.e. the unloading elastic limit defined in Equation (48)); the unloading plastic limit (i.e. while $d_2=b_2$) can be obtained from Equation (51).

As defined previously, due to the additional pressure $p_{20}-p_0$, residual stresses are generated within the cylinder/sphere (i.e. overstrain effect). Subsequently, as the internal pressured is removed, the soil undergoes elastic unloading until the reverse yielding limit $p_{2\mathrm{elim}-2}$ is reached. Based on the shakedown concept, no new plastic deformation will occur in the hollow cylinder/sphere of soil during the subsequent cyclic reloading-unloading under uniform internal pressures varying within the range of ($p_{2\mathrm{elim}-2}$, p_{20}) (neglecting the possible Bauschinger effects) (Hill, 1950; Zhao & Wang, 2010). Providing that the cavity pressure varies in the range of [p_0 , p_{20}], the shakedown limit, within which neither fully plastic state during the initial loading nor reverse plastic state during subsequent unloading will occur in the soil, can be determined by two conditions: (i) $p_{20} \le p_{1\mathrm{plim}}$, and (ii) $p_0 \ge p_{2\mathrm{elim}-2}$, which gives, respectively,

$$p_{20} \le p_0 + \frac{Y + (\alpha - 1) p_0}{\alpha - 1} \left[\left(b_{20} / a_{20} \right)^{k(\alpha-1)/\alpha} - 1 \right] \tag{80}$$

$$p_{20} \le p_0 + \frac{A_1 (\alpha - 1/\alpha) \left(b_{20} / a_{20} \right)^{\frac{k(\alpha-1)}{\alpha}} \left[\left(b_2 / a_2 \right)^{k+1} - 1 \right]}{(\alpha + 1/k) \left(b_2 / a_2 \right)^{k+1} + 1 - \alpha} \tag{81}$$

The shakedown limit equals the minimum value of Equations (80) and (81) as it requires that the inequalities hold simultaneously (Xu & Yu, 2005). It needs to be pointed out that previous shakedown analyses of a hollow cylinder/sphere were mostly carried out in the framework of small strain theory (Hill, 1950; Zhao & Wang, 2010). However, large deformation may occur during the initial elastic-plastic loading process, which may affect the shakedown limit, particularly in soft materials like soils. For example, Yu (1992) observed that the cavity pressure reaches a peak value before the whole cylinder of soil becomes plastic due to the large strain effects, which can also be seen in Figures 8 and 9. Hence, the large strain effects on the shakedown limit are examined by calculating the optimal thickness of hollow cylinders/spheres as follows.

It is known that a hollow cylinder or sphere cannot be too thin to be strengthed (Hill, 1950; Zhao & Wang, 2010). The optimal thickness of a hollow cylinder/sphere for *overstrain* can be determined by taking the equalities of Equation (80) and (81) simultaneously. Within the shakedown limit, the unloading process is purely elastic. Thus, the radial displacement can be determined by Equation (47), from which another relationship between the cavity pressure and the geometry ratio can be obtained as:

$$\frac{b_{20}}{a_{20}} = \frac{b_2}{a_2} \frac{1 - \left[(p_0 - p_{20}) / M \right] \left[(1 + v - kv)(k+1)/k \right] \Big/ \left[(b_2/a_2)^{k+1} - 1 \right]}{1 - \dfrac{p_0 - p_{20}}{M \left[1 - (a_2 / b_2)^{k+1} \right]} \left\{ \left[1 + v - kv - \dfrac{v}{1 - v(2-k)} \right] \left(\dfrac{a_2}{b_2} \right)^{k+1} + \dfrac{v}{1 - v(2-k)} + \dfrac{1 + v - kv}{k} \right\}} \tag{82}$$

Equations (80)-(82) give the value of b_{20}/a_{20} after the *overstrain*, based on which the optimal geometry ratio (i.e. b_0/a_0) can be readily obtained from the displacement solutions of loading (see the Appendix).

At first, the optimal thickness for frictionless soil is investigated. In this special case, the condition of equality of Equations (80)-(81) can be simplified as:

$$\ln\left(b_{20}/a_{20}\right)=\left[2/\left(k+1\right)\right]\left[1-\left(a_2/b_2\right)^{k+1}\right] \tag{83}$$

Equation (83) will reduce to the expression given by Zhao and Wang (2010) for Tresca materials if ideally regarding the surrounding soil as rigid or adopting the small strain definitions (i.e. a_1=a_2=a_0 and b_1=b_2=b_0). However, when the soil deformation during the elastic-plastic loading and elastic unloading process is considered, the optimal thickness will vary with the soil stiffness index G/s_u (s_u represents the shear strength of clay, corresponding to the cohesion strength in the Mohr-Coulomb criterion). The variation of the optimal thickness for both hollow cylinders and spheres with the soil stiffness is presented in Figure 14, taking a broad range of values of G/s_u for clays. It is shown that the optimal thickness decreases with increases of G/s_u and gradually converges to the limit value calculated by Zhao and Wang (2010) for rigid clays. In other words, the geometry changes of the cylinder/sphere during loading and unloading apply insignificant influence on the optimal thickness ratio in stiff clays, whereas this effect cannot be ignored when the soil is relatively soft (e.g. G/s_u<200).

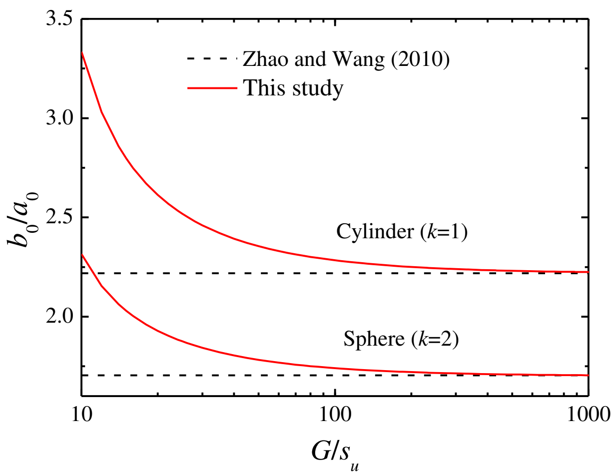

Figure14. Optimal thickness ratio b_0/a_0 of cohesive soil (p_0/s_u=1 and ν=0.5)

For frictional soils, Zhao and Wang (2010) observed that the optimal thickness ratio is a pure function of the friction angle based on the small strain theory. However, Equations (80) and (81) show that it is also dependent on the stiffness and compressibility of materials while taking the geometry changes of the cylinder/sphere into consideration. A selection of results was computed taking the soil cohesion as 0, the Poisson' ratio as 0.3 and the dilation angle as 0 and is plotted in Figure 15. The example results indicate that due consideration should be given to the soil deformation in the shakedown analysis. Its influences on the optimal thickness become greater for a larger value of the friction angle φ and a smaller value of the shear modulus. Not surprisingly, results predicted by the present solution converge to those reported by Zhao and Wang (2010) when the soil is sufficiently stiff (e.g. G/p_0=500 in Figure 15).

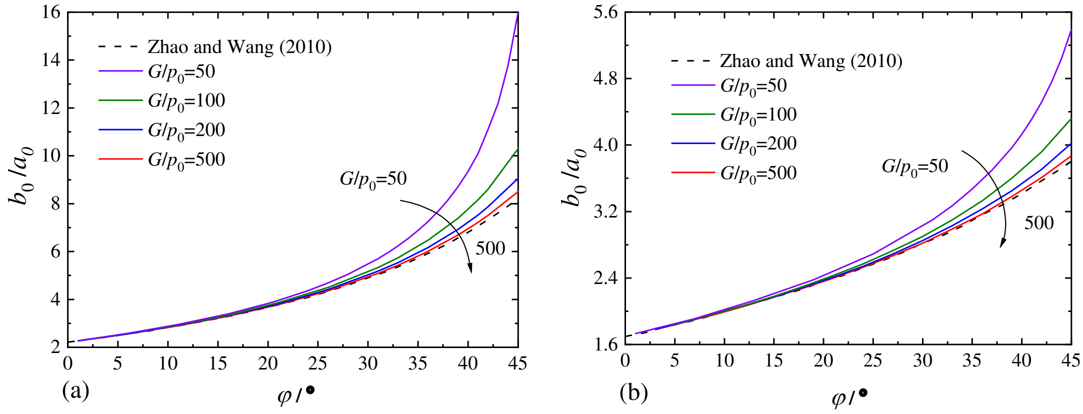

(a) hollow cylinders (b) hollow spheres

Figure15. Optimal thickness ratio b_0/a_0 at various shear moduli and friction angles

Conclusion

This paper presents analytical solutions for quasi-static contraction analysis of a thick-walled cylinder/sphere of dilatant soils. The unloading is assumed to start after an arbitrary magnitude of loading. The logarithmic strain definition is adopted in the plastic zone so that large strain effects are taken into account. A linear elastic perfectly-plastic model is used. The plasticity of the soil is described by adopting the Mohr-Coulomb yield criterion with a non-associated plastic flow rule. The solutions are able to calculate the stress and displacement distribution in the soil at any stage of the unloading process. They are validated by comparing with corresponding analytical solutions for the case of an infinite soil mass. Parametric studies showed that both the reference stress state and the cavity geometry parameters may greatly influence the cavity contraction behaviour, in particular, for thin cylinders and spheres.

The new solutions are useful in modelling many geotechnical problems. Among them, three typical applications are demonstrated, including: preliminary design of the thickness of the frozen cylinder walls under either stress or displacement control, interpretation of laboratory pressuremeter tests with consideration of the finite boundary effect, and determination of the optimal thickness of cylinders/spheres based on the shakedown concept considering large deformation effects. Additionally, the closed-form solutions can also be used to verify elastic-plastic numerical methods in analysing the Mohr-Coulomb materials, in particular, in a finite soil mass.

Disclosure statement

No potential conflict of interest was reported by the authors.

Funding

The work presented in this paper has been supported by the 'Taishan' Youth Scholar Program of Shandong Province, China (No. tsqn201909016, No. tsqn201909044) and 'Qilu' Scholar Program of Shandong University.

References

Abdulhadi, N. O., Germaine, J. T., & Whittle, A. J. (2011). Thick-walled cylinder testing of clays for the study of wellbore instability. *Geotechnical Testing Journal, 34*(6), 746-754

Ajalloeian, R. (1996). *An experimental study of finite pressuremeter length effects in sand.* (PhD), University of Newcastle, Australia.

Ajalloeian, R., & Yu, H. S. (1998). Chamber studies of the effects of pressuremeter geometry on test results in sand. *Géotechnique, 48*(5), 621-636

Alsiny, A., Vardoulakis, I., & Drescher, A. (1992). Deformation localization in cavity inflation experiments on dry sand. *Géotechnique, 42*(3), 395-410

Andersland, O. B., & Ladanyi, B. (2004). *Frozen ground engineering (Second Edition)*. Hoboken, New Jersey: John Wiley & Sons.

Brown, E. T., Bray, J. W., Ladanyi, B., & Hoek, E. (1983). Ground response curves for rock tunnels. *Journal of Geotechnical Engineering, 109*(1), 15-39

Carter, J. (1988). A semi-analytical solution for swelling around a borehole. *International Journal for Numerical and Analytical Methods in Geomechanics, 12*(2), 197-212

Chadwick, P. (1959). The quasi-static expansion of a spherical cavity in metals and ideal soils. *The Quarterly Journal of Mechanics and Applied Mathematics, 12*(1), 52-71

Chen, S. L., & Abousleiman, Y. N. (2016). Drained and undrained analyses of cylindrical cavity contractions by bounding surface plasticity. *Canadian Geotechnical Journal, 53*(9), 1398-1411

Chen, S. L., Abousleiman, Y. N., & Muraleetharan, K. K. (2012). Closed-form elastoplastic solution for the wellbore problem in strain hardening/softening rock formations. *International Journal of Geomechanics, 12*(4), 494-507

Cheng, Y., & Yang, H.-W. (2019). Exact solution for drained spherical cavity expansion in saturated soils of finite radial extent. *International Journal for Numerical and Analytical Methods in Geomechanics, 43*, 1594–1611. doi: doi: org/10.1002/nag.2924

Clarke, B. G. (1995). *Pressuremeters in geotechnical design*. London: Blackie Academic & Professional.

Collins, I. F., & Yu, H. S. (1996). Undrained cavity expansions in critical state soils. *International Journal for Numerical and Analytical Methods in Geomechanics, 20*(7), 489-516

Fahey, M. (1986). Expansion of a thick cylinder of sand: a laboratory simulation of the pressuremeter test. *Geotechnique, 36*(3), 397-424

Fahey, M., & Carter, J. P. (1993). A finite element study of the pressuremeter test in sand using a nonlinear elastic plastic model. *Canadian Geotechnical Journal, 30*(2), 348-362

Ferreira, R., & Robertson, P. (1992). Interpretation of undrained self-boring pressuremeter test results incorporating unloading. *Canadian Geotechnical Journal, 29*(6), 918-928

Franza, A., Marshall, A., & Zhou, B. (2019). Greenfield tunnelling in sands: the effects of soil density and relative depth. *Géotechnique, 69*(4), 297-307. doi: doi: org/10.1680/jgeot.17.P.091

Gao, X. L., Wen, J. F., Xuan, F.-Z., & Tu, S. T. (2015). Autofrettage and Shakedown Analyses of an Internally Pressurized Thick-Walled Cylinder Based on Strain Gradient Plasticity Solutions. *Journal of Applied Mechanics, 82*(4), 041010

Geng, Y., Yu, H. S., & McDowell, G. R. (2012). Discrete element modelling of cavity expansion and pressuremeter test. *Geomechanics and Geoengineering, 8*(3), 179-190. doi: doi: org/10.1080/17486025.2012.735375

Ghionna, V. N., & Jamiolkowski, M. (1991). A critical appraisal of calibration chamber testing of sands *the First International Symposium on Calibration Chamber Testing* (pp. 13-40). Potsdam, New York: Elsevier.

Grant, R. J. (1998). *Movements around a tunnel in two-layer ground.* (PhD thesis), City University London, London.

Hill, R. (1950). *The mathematical theory of plasticity*. London: Oxford University Press.

Houlsby, G. T., & Carter, J. P. (1993). The effects of pressuremeter geometry on the results of tests in clay. *Géotechnique, 43*(4), 567-576

Houlsby, G. T., Clarke, B. G., & Wroth, C. P. (1985). Analysis of the unloading of a pressuremeter in sand *the 2nd International Symposium on The Pressuremeter and its Marine Applications* (pp. 245-262). West Conshohocken, PA: ASTM International.

Houlsby, G. T., & Withers, N. J. (1988). Analysis of the cone pressuremeter test in clay. *Géotechnique, 38*(4), 575-587

Hughes, J. M. O., & Robertson, P. K. (1985). Full-displacement pressuremeter testing in sand. *Canadian Geotechnical Journal, 22*(3), 298-307

Hughes, J. M. O., Wroth, C. P., & Windle, D. (1977). Pressuremeter tests in sands. *Géotechnique, 27*(4), 455-477

Jefferies, M. G. (1988). Determination of horizontal geostatic stress in clay with self-bored pressuremeter. *Canadian Geotechnical Journal, 25*(3), 559-573

Jewell, R., Fahey, M., & Wroth, C. (1980). Laboratory studies of the pressuremeter test in sand. *Geotechnique, 30*(4), 507-531

Jirari, S. E., Wong, H., Deleruyelle, F., Branque, D., Berthoz, N., & Leo, C. (2020). Analytical modelling of a tunnel accounting for elastoplastic unloading and reloading with reverse yielding and plastic flow. *Computers and Geotechnics, 121*, 103441. doi: doi.org/10.1016/j.compgeo.2020.103441

Juran, I., & BenSaid, M. (1987). Cavity expansion tests in a hollow cylinder cell. *Geotechnical Testing Journal, 10*(4), 203-212

Klein, J., & Gerthold, A. (1979). Die Fliessbedingung von Drucker/Prager im Vergleich zu anderen Bruchkriterien bei der Bemessung von Gefrierschächten. *Bautechnik, 11*(1979), 368-375

Mair, R. J. (1979). *Centrifugal modelling of tunnel construction in soft clay.* (PhD thesis), Cambridge University, Cambridge, UK.

Mair, R. J., & Taylor, R. N. (1993). Prediction of clay behaviour around tunnels using plasticity solutions *Predictive Soil Mechanics: Proceedings of the Wroth Memorial Symposium* (pp. 449-463). Oxford, UK: Thomas Telford.

Mair, R. J., & Wood, D. M. (1987). *Pressuremeter testing: methods and interpretation*. London, UK: CIRIA-Butterworths.

Manassero, M. (1989). Stress-strain relationships from drained self-boring pressuremeter tests in sand. *Geotechnique, 39*(2), 293-307

Mo, P. Q., & Yu, H. S. (2017). Undrained Cavity-Contraction Analysis for Prediction of Soil Behavior around Tunnels. *International Journal of Geomechanics, 17*(5), 04016121-04016121-04016110. doi: DOI: 10.1061/(ASCE)GM.1943-5622.0000816.

Ogawa, T., & Lo, K. Y. (1987). Effects of dilatancy and yield criteria on displacements around tunnels. *Canadian Geotechnical Journal, 24*(1), 100-113

Park, K. H. (2014). Similarity solution for a spherical or circular opening in elastic-strain softening rock mass. *International Journal of Rock Mechanics and Mining Sciences, 71*, 151-159

Pournaghiazar, M., Russell, A. R., & Khalili, N. (2013). Drained cavity expansions in soils of finite radial extent subjected to two boundary conditions. *International Journal for Numerical and Analytical Methods in Geomechanics, 37*(4), 331-352

Reed, M. B. (1986). Stresses and displacements around a cylindrical cavity in soft rock. *IMA Journal of Applied Mathematics, 36*(3), 223-245

Rowe, P. W. (1962). The stress-dilatancy relation for static equilibrium of an assembly of particles in contact *the royal society of London a: mathematical, physical and engineering sciences* (Vol. 269, pp. 500-527): The Royal Society.

Salgado, R., Mitchell, J. K., & Jamiolkowski, M. (1998). Calibration chamber size effects on penetration resistance in sand. *Journal of Geotechnical and Geoenvironmental Engineering, 124*(9), 878-888

Sanger, F., & Sayles, F. (1979). Thermal and rheological computations for artificially frozen ground construction. *Engineering geology, 13*(1-4), 311-337

Schnaid, F., & Houlsby, G. (1991). An assessment of chamber size effects in the calibration of in situ tests in sand. *Geotechnique, 41*(3), 437-445

Schnaid, F., & Houlsby, G. (1992). Measurement of the properties of sand by the cone pressuremeter test. *Géotechnique, 42*(4), 587-601

Schnaid, F., Ortigao, J. A., Mantaras, F., Cunha, R., & MacGregor, I. (2000). Analysis of self-boring pressuremeter (SBPM) and Marchetti dilatometer (DMT) tests in granite saprolites. *Canadian geotechnical journal, 37*(4), 796-810

Sharan, S. K. (2008). Analytical solutions for stresses and displacements around a circular opening in a generalized Hoek–Brown rock. *International Journal of Rock Mechanics and Mining Sciences, 1*(45), 78-85

Shuttle, D. (2007). Cylindrical cavity expansion and contraction in Tresca soil.

Géotechnique, 57(3), 305-308

Viggiani, G., & Casini, F. (2015). Artificial ground freezing: from applications and case studies to fundamental research *the XVI ECSMGE: Geotechnical Engineering for Infrastructure and Development* (pp. 65-92). Edinburgh.

Vrakas, A., & Anagnostou, G. (2014). A finite strain closed-form solution for the elastoplastic ground response curve in tunnelling. *International Journal for Numerical and Analytical Methods in Geomechanics, 38*(11), 1131-1148

Wen, J.-F., Gao, X.-L., Xuan, F.-Z., & Tu, S.-T. (2017). Autofrettage and shakedown analyses of an internally pressurized thick-walled spherical shell based on two strain gradient plasticity solutions. *Acta Mechanica, 228*(1), 89-105

Withers, N., Howie, J., Hughes, J., & Robinson, P. (1989). Performance and analysis of cone pressuremeter tests in sands. *Geotechnique, 39*(3), 433-454

Wroth, C. (1982). British experience with the self-boring pressuremeter *the 1st International Symposium on The Pressuremeter and its Marine Applications* (pp. 143-164). Paris.

Wroth, C. P. (1984). The interpretation of in situ soil tests. *Géotechnique, 34*(4), 449-489

Xu, S. Q., & Yu, M. H. (2005). Shakedown analysis of thick-walled cylinders subjected to internal pressure with the unified strength criterion. *International journal of pressure vessels and piping, 82*(9), 706-712

Yu, H. S. (1992). Expansion of a thick cylinder of soils. *Computers and Geotechnics, 14*(1), 21-41

Yu, H. S. (1993). Finite elastoplastic deformation of an internally pressurized hollow sphere. *Acta Mechaniea Solida Sinica (English Edition), 6*(1), 81–97

Yu, H. S. (1994). State parameter from self-boring pressuremeter tests in sand. *Journal of geotechnical engineering, 120*(12), 2118-2135

Yu, H. S. (1996). Interpretation of pressuremeter unloading tests in sands. *Géotechnique, 46*(1), 17-31

Yu, H. S. (2000). *Cavity expansion methods in geomechanics*. Dordrecht, the Netherlands: Kluwer Academic Publishers.

Yu, H. S., & Houlsby, G. T. (1991). Finite cavity expansion in dilatant soils: loading analysis. *Géotechnique, 41*(2), 173-183

Yu, H. S., & Houlsby, G. T. (1995). A large strain analytical solution for cavity contraction in dilatant soils. *International Journal for Numerical and Analytical Methods in Geomechanics, 19*(11), 793-811

Yu, H. S., & Rowe, R. K. (1999). Plasticity solutions for soil behaviour around contracting cavities and tunnels. *International Journal for Numerical and Analytical Methods in Geomechanics, 23*(12), 1245-1279

Yu, H. S., Zhuang, P. Z., & Mo, P. Q. (2019). A unified critical state model for geomaterials with an application to tunnelling. *Journal of Rock Mechanics and Geotechnical Engineering, 11*(3), 464-480. doi: org/10.1016/j.jrmge.2018.09.004

Zhang, B., Yang, W., & Wang, B. (2018). Plastic Design Theory of Frozen Wall Thickness in an Ultradeep Soil Layer Considering Large Deformation Characteristics. *Mathematical Problems in Engineering, 2018*, 8513413. doi: doi: org/10.1155/2018/8513413

Zhao, J., & Wang, G. (2010). Unloading and reverse yielding of a finite cavity in a bounded cohesive–frictional medium. *Computers and Geotechnics, 37*(1), 239-245

Appendix

At the moment that the elastic-plastic boundary reaches the outer radius of the cavity upon loading, the displacement at $r=b_{20}$ can be calculated from the elastic displacement solution of Yu (1992, 1993) as:

$$b_0 = b_{20}\left\{1-\frac{(1+v-kv)\left[Y+(\alpha-1)p_0\right]}{M\alpha}\right\} \tag{84}$$

The displacement of the inner wall of the cavity (i.e. $r=a_{20}$) can be obtained from the large strain plastic displacement solution as below.

$$\sum_{n=0}^{\infty}\Omega_n^4 = \frac{\bar{\eta}}{\bar{\gamma}}\left[\left(\frac{b_0}{b_{20}}\right)^{\frac{k}{\beta}+1} - \left(\frac{a_0}{b_{20}}\right)^{\frac{k}{\beta}+1}\right] \tag{85}$$

in which $\bar{\gamma} = \dfrac{(k+\beta)\alpha}{k\beta(\alpha-1)}$, and

$$\Omega_n^4 = \begin{cases} \dfrac{k(\alpha-1)\omega_3^n}{\alpha n!}\ln\dfrac{b_{20}}{a_{20}} & \text{, if } n=\bar{\gamma} \\ \dfrac{\omega_3^n}{(n-\bar{\gamma})n!}\left[(b_{20}/a_{20})^{\frac{k(\alpha-1)(n-\bar{\gamma})}{\alpha}}-1\right] & \text{, otherwise} \end{cases} \tag{86}$$

$$\omega_3 = \frac{Y + (\alpha - 1) p_0}{M\beta(\alpha-1)\alpha}\left[\alpha\beta - \frac{\alpha k v}{1 - v(2-k)} + k(1 + v - kv) - k\beta \frac{v}{1 - v(2-k)}\right] \tag{87}$$

$$\ln \overline{\eta} = \frac{Y + (\alpha - 1) p_0}{M\beta(\alpha-1)}\left[\beta - \frac{k v}{1 - v(2-k)} + k(1 + v - kv) - \frac{k\beta v}{1 - v(2-k)}\right] \tag{88}$$

Notation

a_0, b_0	initial inner and outer radii of a cylinder/sphere
p_0, p_{20}	in-situ stress and cavity pressure at the beginning of unloading
p_{in}	internal cavity pressure
a_{20}, b_{20}	initial inner and outer radii of a cylinder/sphere at the beginning of unloading
k	k=1 for a cylinder and k=2 for a sphere
r, θ, z	cylindrical polar coordinates
r, θ, ϕ	spherical polar coordinates
σ_r, σ_θ, σ_z	radial, circumferential and axial stresses
$\Delta\sigma_r$, $\Delta\sigma_\theta$	incremental radial and circumferential stresses due to unloading
u_{20}, u_2	radial displacement at the beginning of unloading and during unloading
Δu	incremental radial displacement due to unloading
σ_{r2}, $\sigma_{\theta 2}$	radial and circumferential stresses during unloading
σ_{r20}, $\sigma_{\theta 20}$	radial and circumferential stresses at the beginning of unloading
r_0	initial radius of a given soil particle
a_2, b_2	inner and outer radii of the cavity during unloading
p_1, p_2	internal cavity pressures during loading and unloading
c_1, c_{20}, c_2	radii of the elastic-plastic interface caused by loading in the loading process, at the end of loading and during unloading
d_2, d_{20}	radius of the elastic-plastic interface caused by unloading and its initial value
φ, c, ψ	soil friction angle, cohesion and dilation angle
α, Y	functions of soil cohesion and friction angle
β	function of dilation angle
$p_{1\mathrm{elim}}$	elastic limit pressure in the loading process

a_1, b_1	inner and outer radii of a cavity in the loading process
r_1, r_2	radial radii during loading and unloading
σ_{r1}, $\sigma_{\theta 1}$	radial and circumferential stresses during loading
A_1, B_1	constants of integration in the loading process
ε_r, ε_θ	radial and circumferential strains
v, E, G	Poisson's ratio, elastic modulus and shear modulus
M	function of Poisson's ratio and elastic modulus
a_2, b_2	inner and outer radii of a cavity in the unloading process
$p_{2\text{elim-1}}$	elastic unloading limit of case I
$A_{2\text{-}1}$, $B_{2\text{-}1}$	constants of integration in the unloading process of case I
$p_{2\text{fp-lim}}$	fully plastic unloading limit of case I
ε_r^p, ε_θ^p	plastic radial and circumferential strains
ε_r^e, ε_θ^e	elastic radial and circumferential strains
η, ω, θ, γ	non-dimensional coefficients of case I
$n!$	factorial of n
$A_{2\text{-}1}$, $B_{2\text{-}1}$, $A_{2\text{-}2}$, $B_{2\text{-}2}$, $A_{2\text{-}3}$, $B_{2\text{-}3}$, $A_{2\text{-}4}$, $A_{2\text{-}5}$	constants of integration in the unloading process
$p_{2\text{elim-2}}$	elastic unloading limit of cases II and III
$\Delta\varepsilon_r$, $\Delta\varepsilon_\theta$	incremental radial and circumferential strains due to unloading
ω_1, λ_1, $\overline{\theta}$, ρ	non-dimensional coefficients of case II
Ω_n^1, Ω_n^2, Ω_n^3, Ω_n^4	infinite power series
η_1, ω_2, λ_2	non-dimensional coefficients of case III
L, D	length and diameter of pressuremeters
D_r	relative density of sand
φ_{cv}, φ_{ps}, φ_{tri}	critical state friction angle, plane strain friction angle and

	triaxial friction angle of sand
R^2	the correlation coefficient
$p_{1\mathrm{plim}}$	plastic limit during loading
s_u	shear strength of clay
$\overline{\eta}$, ω_3, $\overline{\gamma}$	non-dimensional coefficients in Appendix